HHS Public Access

Author manuscript

Dev Cell. Author manuscript; available in PMC 2019 April 23.

Published in final edited form as:

Dev Cell. 2018 April 23; 45(2): 226–244.e8. doi:10.1016/j.devcel.2018.03.020.

Ari-1 regulates myonuclear organization together with Parkin and is associated with aortic aneurysms

Kai Li Tan[1,#], **Nele A. Haelterman**[1,2,#], **Callie S. Kwartler**[3], **Ellen S. Regalado**[3], **Pei-Tseng Lee**[2], **Sonal Nagarkar-Jaiswal**[2,4], **Dong-chuan Guo**[3], **Lita Duraine**[4], **Michael F. Wangler**[1,2], **University of Washington Center for Mendelian Genomics**[4], **Michael J. Bamshad**[5], **Deborah A. Nickerson**[5], **Guang Lin**[2], **Dianna M. Milewicz**[3], and **Hugo J. Bellen**[1,2,4,6,7,*]

[1]Program in Developmental Biology, Baylor College of Medicine, Houston, TX, 77030, USA

[2]Department of Molecular and Human Genetics, Baylor College of Medicine (BCM), Houston, TX, 77030, USA

[3]Department of Internal Medicine, The University of Texas Health Science Center at Houston McGovern Medical School, Houston, TX, 77030, USA

[4]Howard Hughes Medical Institute, BCM, Houston, TX, 77030, USA

[5]Department of Genome Sciences, University of Washington, Seattle, WA 98195, USA

[6]Jan and Dan Duncan Neurological Research Institute, Texas Children's Hospital (TCH), Houston, TX, 77030, USA

[7]Department of Neuroscience, BCM, Houston, TX, 77030, USA

Summary

Nuclei are actively positioned and anchored to the cytoskeleton via the LINC (LInker of Nucleoskeleton and Cytoskeleton) complex. We identified mutations in the Parkin-like E3 ubiquitin ligase Ariadne-1 (Ari-1) that affect the localization and distribution of LINC complex members in *Drosophila. ari-1* mutants exhibit nuclear clustering and morphology defects in larval muscles. We show that Ari-1 mono-ubiquitinates the core LINC complex member Koi. Surprisingly, we discovered functional redundancy between Parkin and Ari-1: increasing Parkin expression rescues *ari-1* mutant phenotypes and vice versa. We further show that rare variants in

*Corresponding author: Hugo J. Bellen at hbellen@bcm.edu.
#Equal contribution
Lead contact: Hugo J. Bellen at hbellen@bcm.edu

Author Contributions

K.L.T., N.A.H., D.M.M. and H.J.B. designed the study. K.L.T. and N.A.H. performed molecular genetics and animal modeling studies. E.S.R., D.G. and D.M.M. recruited patients, collected clinical information and samples. M.J.W., UW-CMG, M.J.B. and D.A.N. performed genomic analyses. G.L. provided advice on *in vitro* experiments. K.L.T., N.A.H. and C.S.K performed human smooth muscle cell experiments. K.L.T., N.A.H. and H.J.B wrote the manuscript, which was revised and approved by all authors. D.M.M. and H.J.B. obtained funding for and supervised the study.

Competing financial interest

The authors declare no competing financial interests.

the human homolog of *ari-1* (*ARIH1*) are associated with thoracic aortic aneurysms and dissections, conditions resulting from smooth muscle cell (SMC) dysfunction. Human *ARIH1* rescues fly *ari-1* mutant phenotypes, whereas human variants found in patients fail to do so. In addition, SMCs obtained from patients display aberrant nuclear morphology. Hence, ARIH1 is critical in anchoring myonuclei to the cytoskeleton.

TOC image

The Parkin-like E3 ligase Ari-1 regulates physical connection between nuclei and the cytoskeleton. Tan and Haelterman et al. show that Ari-1 acts through the LINC complex to affect nuclear organization and shape in striated muscles. Human Ari-1 mutations similar phenotypes in vascular smooth muscle, and are associated with aortic aneurysms.

Subject terms

Drosophila; ring in between ring E3 ligases; Linker of Nuclear skeleton and Cytoskeleton (LINC); human genetics; ARIH1; MSP300; Koi; KASH; SUN proteins; aortic dissection; nuclear envelope

Introduction

Localization of a nucleus in a specific subcellular location is a highly regulated and dynamic process. Depending on the cell type, nuclear localization can affect cell division and differentiation (Kim et al., 2015, Spear and Erickson, 2012), cell migration (Foe and Alberts, 1983, Kim et al., 2014) or cellular function. In humans, loss of proper nuclear positioning has been implicated in muscular dystrophy (Folker and Baylies, 2013), lissencephaly (Koizumi et al., 2006), cerebellar ataxia (Gros-Louis et al., 2007) and deafness (Horn et al., 2013). The LINC complex is required for proper nuclear localization and consists of various proteins – Lamins, SUN (Sad1 and UNc84 homology proteins) and KASH (Klarsicht, ANC-1, and Syne Homology) proteins – that cross the nuclear envelope and project into the cytoplasm to connect the nucleoskeleton to the cytoskeletal network (Bone and Starr, 2016). Lamins, the main component of the nuclear lamina, interact with SUN proteins that cross the inner nuclear membrane into the perinuclear space (Figure S1A). Within the perinuclear space, the SUN domain interacts with the C-terminus of KASH proteins that in turn span the outer nuclear membrane and interact with various members of the cytoskeleton. Apart from placing a nucleus in its appropriate position in the cell, the LINC complex also endows a cell with the ability to respond to changes in its micro-environment, such as changes in cell shape or migration. This process was recently dubbed nuclear mechanosensing (Navarro et al., 2016). External stimuli that alter cell shape introduce mechanical tension on the plasma membrane, which is transferred through the cytoskeleton and the LINC complex to alter nuclear morphology and/or transcription (Neelam et al., 2015, Arsenovic et al., 2016). This suggests that the LINC complex is required for mechanosensing, an important feature for cells, in particular muscle cells that have to respond to constant changes in mechanical forces that are applied to them (Volk and Wang, 2015).

Some of the LINC complex components have been shown to be the subject of few posttranslational modifications (Simon and Wilson, 2013). However, a role for

ubiquitination in the regulation of the LINC complex has not been documented so far. The human genome encodes ~700 E3 ligases, 14 of which are RING-between-RING (RBR) ligases (Deshaies and Joazeiro, 2009, Eisenhaber et al., 2007). The best-known member of the RBR family in *Drosophila* is encoded by the *parkin* locus, because mutations in human *PARK2* (*parkin*) cause a recessive form of early onset Parkinson's disease (Lucking et al., 2000). Parkin plays a role in clearing dysfunctional mitochondria based on fly mutants (Pesah et al., 2004, Greene et al., 2003, Narendra et al., 2008) and mammalian cell culture experiments (Geisler et al., 2010), but numerous mouse knock outs of *Park2* have revealed little about the protein's *in vivo* function in mice (Stephenson et al., 2012). Much less is known about the other members of the RBR family of E3 ligases. The human homolog of Ari-1 (ARIH1) was recently shown to function together with Cullins of the RING family of E3 ligases to regulate several cell cycle regulators (Scott et al., 2016). In this setting, ARIH1 transfers the first ubiquitin molecule to the Cullin substrate, upon which Cullin lengthens the poly-ubiquitin chain. In flies, Ari-1 was shown to be an essential protein that can dimerize and can regulate the insect hormonal ecdysone signaling pathway (Aguilera et al., 2000, Gradilla et al., 2011).

Interestingly, although Parkin and Ari-1 are thought to have unique biological functions, the two proteins are similar at the structural level and Ari-1 interacts with a subset of established Parkin substrates (Parelkar et al., 2012). In addition, both proteins are activated by the same E2 conjugating enzyme, UbcD10 (fly)/UBCH7 (human) (Wenzel et al., 2011, Aguilera et al., 2000).

We identified lethal mutations in *ari-1* from an X-chromosome mutagenesis screen in *Drosophila* (Haelterman et al., 2014a, Yamamoto et al., 2014). Phenotypic characterization of the mutants revealed a role for Ari-1 in positioning nuclei in muscles by regulating the LINC complex. We show that Ari-1 mono-ubiquitinates Koi. In the absence of Ari-1, Parkin can partially compensate for the loss of Ari-1 and vice-versa. In contrast, *ari-1* missense mutations act in a dominant negative fashion and the mutant forms of Ari-1 affect Parkin, inhibiting its function in nuclear positioning. Furthermore, we identified three variants of *ARIH1* in patients with aortic or cerebrovascular aneurysms. Aortic tissues from these patients reveal that vascular smooth muscle cell (vSMC) nuclear morphology is severely affected. Further testing of the identified *ARIH1* variants in *Drosophila* show that the mutant forms of *ARIH1* are less- or non-functional. In sum, we have identified an evolutionarily conserved role of Ari-1/ARIH1 with Parkin in regulating myonucleo-cytoskeletal anchorage and shape, and variants in *ARIH1* are associated with developing aortic aneurysms in humans.

Results

Loss of *ari-1* causes pleiotropic phenotypes that are rescued by human ARIH1

To identify essential genes on the *Drosophila* X-chromosome that affect neural development and neuronal maintenance, we previously performed a large-scale forward genetic mutagenesis screen (Haelterman et al., 2014a, Yamamoto et al., 2014). From this screen, we isolated three alleles that form a complementation group (Figure 1A). These alleles ($ari\text{-}1^{A}$, $ari\text{-}1^{B}$ and $ari\text{-}1^{D}$) cause late pupal lethality and exhibit pleiotropic phenotypes (Figure S1B).

Mosaic analysis using the FLP-FRT system allowed the generation of large homozygous mutant clones in various tissues (Figure S1B). Electroretinograms (ERGs) of cells in mutant eye clones showed a synaptic transmission defect (Figure S1B). In addition, adult escapers have thinner bristles (Figure S1B) and reduced lifespan (Figure S1C). These findings are consistent with previously described phenotypes associated with *ari-1* mutants which are no longer available (Aguilera et al., 2000).

The three novel alleles, *ari-1*^{A}, *ari-1*^{B} and *ari-1*^{D}, contain missense mutations that alter evolutionarily conserved amino acids (Figure 1A). Lethality and lifespan of the mutants are rescued by a genomic Pacman construct, which is a BAC clone that contains an 80kb genomic region encompassing *ari-1* (GR: indicates the presence of two copies of the genomic rescue construct) (Venken et al., 2006). Moreover, ubiquitous expression (da-GAL4) of *ari-1's* human homologue, *ARIH1* (Figure 1C and Figure S1C), rescues the lethality in *ari-1* missense mutants. Lethality cannot be rescued by neuronal (*nSyb>ARIH1*) or muscle (*C57* or *Mef>ARIH1)* specific expression.

Given that the EMS-induced alleles are missense mutations, we generated a null allele to ensure that the studied phenotypes are truly attributable to loss of *ari-1*. To this end, we integrated a modified Mi{MIC}-like cassette into the genome of a wildtype animal, using CRISPR technology with homologous recombination (Figure S2A–B). We designed the CRI{MIC} cassette based on the properties of the exchangeable gene-trap cassette that is present in the Mi{MIC} transposon (Venken et al., 2011). As shown in Figure 1B, it contains a splice acceptor followed by a polyadenylation signal as well as translational stop codons in all three reading frames and a dominant eye marker (RNAi against *white*). We integrated the CRI{MIC} cassette in the first coding intron (located between the first and second coding exon) of *ari-1* (Figure 1B and Figure S2B). The CRI{MIC} cassette introduces a transcriptional stop in the first coding intron and none of the subsequent exons are detectable by QRT-PCR (Figure S1D), suggesting that it is a null allele. Similar to the other *ari-1* alleles, *ari-1*$^{CRi\{MIC\}}$ is recessive lethal (Figure 1A), the mutants die as pharate pupae and fail to complement the lethality of the other alleles.

To determine the expression pattern and subcellular localization of Ari-1, we used a previously generated antibody (Gradilla et al., 2011), but were unable to detect the protein. We therefore performed recombination mediated cassette exchange (RMCE) on *ari-1*$^{CRi\{MIC\}}$ to exchange the gene trap for an artificial exon that contains various tags, including GFP (GFSTF) (Figure 1B)(Nagarkar-Jaiswal et al., 2015b, Venken et al., 2011). We successfully tagged Ari-1 (*ari-1*$^{CRI\{GFSTF\}}$, Figure 1B), and this reverted the lethality and much reduced longevity of *ari-1*$^{CRi\{MIC\}}$ (Figure 1A, C and Figure S1C), showing that Ari-1$^{CRI\{GFSTF\}}$ is a functional protein. Western blot and GFP-pulldown of Ari-1$^{CRI\{GFSTF\}}$ allow the detection of a band of the expected size (around 86kD) (Figure S2C). Unfortunately, the protein levels of Ari-1$^{CRI\{GFSTF\}}$ in live or fixed animals are below the detection limit for immunostaining. Similarly, using the previously generated Ari-1 antibody (Gradilla et al., 2011), we were unable to detect endogenous Ari-1. Hence, Ari-1 is likely expressed at low levels, or the tags are masked. To determine the expression pattern of Ari-1, we generated *ari-1*$^{CRI\{T2A\text{-}GAL4\}}$ via RMCE of *ari-1*$^{CRi\{MIC\}}$ to replace the CRI{MIC} cassette with a T2A-GAL4 cassette (Figure 1B). The T2A cassette contains a splice acceptor

and a viral T2A peptide sequence, which induces the ribosome to skip the penultimate peptide bond but reinitiates translation at the GAL4 sequence. The latter can be used to drive the expression of UAS-2×GFP (Gnerer et al., 2015, Diao et al., 2015), revealing that Ari-1 is expressed ubiquitously, including in muscles (Figure S2D).

To compare the phenotypes of *ari-1* missense mutants to the null mutant (*ari-1*$^{CRi\{MIC\}}$), we examined lethal phases. No adult homozygous/hemizygous animals are observed when all progeny is kept in the same vial. However, when mutants are reared separately, about 50% of the hemizygous *ari-1*$^{CRi\{MIC\}}$ mutant animals eclose, whereas only 3% of the missense mutant animals eclose (Figure 1C). Note that the *ari-1*^{mutant} escapers are unable to fly or climb and only live 2–3 days (Figure S1C). The lethality in *ari-1*$^{CRi\{MIC\}}$ mutants is due to loss of *ari-1*, as viability is fully restored by the GR (Figure 1A and C). In summary, loss of Ari-1 is associated with a weaker phenotype than the three missense mutations. Interestingly, reducing the amount of the missense mutant protein by generating *ari-1*^{A}, *ari-1*^{B} or *ari-1*^{D} / *deficiency* (*def*) flies leads to significantly more escapers than any of the homozygous or transheterozygous combinations (Figure 1C). These data indicate that the presence of a missense mutation in Ari-1 is more severely affecting certain processes than absence of the protein.

Ari-1 controls shape and subcellular localization of nuclei in *Drosophila* larval muscles

Phenotypic analyses of *ari-1* mutants revealed aberrant nuclear spacing in striated muscles. In wildtype larvae, myonuclei are evenly spaced within multinucleated striatal muscles (Figure 1D–E) and can rarely be seen to cluster together or contact each other. In contrast, contacting nuclei can be observed in about 60% of the *ari-1* mutant muscles (segment 3, muscle 6) (Figure 1D–E). This defect is not caused by an increased number of myonuclei (Figure S3A). *ari-1*$^{CRI\{MIC\}}$ null mutants show a less severe myonuclear defect than the missense mutants (Figure 1D–E), similar to lethality (Figure 1C). Note that the nuclear positioning phenotype observed in *ari-1*$^{CRI\{MIC\}}$ mutants is reverted when the gene trap is exchanged for a protein trap (*ari-1*$^{\{GFSTF\}}$), demonstrating that the phenotypes are indeed due to loss of *ari-1* (Figure 1E).

To explore why missense mutations cause a more severe phenotype than the *ari-1*$^{CRI\{MIC\}}$ null allele (Figure 1E; green), we assessed dominance and showed that *ari-1*$^{A\ or\ B\ or\ D}$ / *wildtype* (*wt*) animals, although having normal lifespan (Figure S3B), display defects in nuclear positioning (Figure 1E; brown). The phenotype of *ari-1*$^{A\ or\ B\ or\ D}$/*wt* animals is less severe than those observed in hemizygous missense mutants (Figure 1E; green), showing that these three alleles are semi-dominant. The phenotype in missense mutants is due to a loss, rather than an increase or a novel function of Ari-1, since introducing the GR strongly suppresses nuclear clustering defects (Figure 1E; compare green versus blue). In addition, muscle-specific expression of wildtype *ari-1* (*Mef>ari-1*), in *ari-1*$^{A\ or\ B\ or\ D}$ fully suppresses the phenotype (Figure 1E; yellow). The latter two observations are the genetic hallmarks of dominant negative mutations. Together, our data indicate that (1) Ari-1 functions cell-autonomously, (2) the missense mutations behave as dominant negative alleles, and (3) the nuclear positioning defects are due to mutations in *ari-1*. Moreover, the observation that the

null allele is less severe than the missense alleles, suggests that another partially redundant protein may compensate for the absence of *ari-1*.

While analyzing nuclear spacing, we also noticed that myonuclear morphology is aberrant in *ari-1* mutants. LaminC antibody staining, marking the nuclear envelope, reveals circular and smooth nuclei that have an even distribution of LaminC in wild type cells (Figure 2A). In contrast, in *ari-1* mutants, nuclear size is decreased, and the nuclear envelope appears uneven, with indentations and lamin foci (Figure 2A and S3C). Transmission electron microscopy (TEM) of third instar larval muscles revealed that wildtype and $ari\text{-}1^{mutant}; GR$ muscle nuclei have an ellipsoid shape, reside close to the cell surface and are surrounded by the muscle cytoskeletal network or mitochondria (Figure 2B). In *ari-1* mutants, however, the nuclear envelope is uneven (Figure 2B), nuclei are displaced from the cell membrane, and there appears to be no cytoskeletal network surrounding the nuclei (Figure 2B). Immunostaining data shows that the network of microtubules that normally surround myonuclei is much reduced in *ari-1* mutants, a phenotype that was also observed in LINC complex mutants (Figure S3D)(Elhanany-Tamir et al., 2012). In summary, these results suggest that the nuclei have lost their nucleo-cytoskeletal coupling and have become disconnected from the plasma membrane.

Ari-1 controls the LINC complex and ubiquitinates Koi, a member of the LINC complex

To assess how Ari-1 regulates nuclear positioning, we focused on the LINC complex (Bone and Starr, 2016). This complex determines the subcellular localization of a nucleus by providing nucleo-cytoskeletal coupling (Figure S1A)(Chang et al., 2015). The *Drosophila* genome encodes two KASH proteins, Msp-300 and Klarsicht, as well as two SUN proteins, Spag4 and Klaroid (Koi). Spag4 is only expressed in testes (Kracklauer et al., 2010). To determine the expression of Koi, we used $koi^{P\{PTT\}}$ a protein trap that expresses GFP-tagged Koi (Figure S3E)(Buszczak et al., 2007). Immunostaining revealed that Koi is ubiquitously expressed and localizes to the nuclear envelope (Figure S3E). Both KASH proteins (Msp-300 and Klarsicht) are required for proper myonuclear positioning (Figure S3F) (Elhanany-Tamir et al., 2012), but no muscle phenotype has been documented for the loss of Koi. As shown in Figure S3F, $koi^{84/Def}$ mutants display a strong nuclear clustering phenotype with 100% penetrance. Hence, in muscles, myonuclear positioning is determined by LINC complexes that consist of the KASH proteins Klarsicht and Msp-300, as well as the SUN protein Koi.

To determine if the LINC complex is altered in *ari-1* mutants, we performed immunostaining for KASH and SUN proteins. The subcellular localization of Msp-300 is obviously altered in *ari-1* mutants. Msp-300 localizes to the nuclear envelope and Z-discs in control and GR muscles (Figure 3A)(Elhanany-Tamir et al., 2012) but in *ari-1* mutants, Msp-300 proteins are mislocalized and detached from the nuclear envelope (Figure 3A). In addition, immunostaining and western blots for Koi revealed an increase in Koi both in total protein levels and at the nuclear envelope of *ari-1* mutants (Figure 3B–C). In contrast, the mRNA levels of both Koi and Msp-300 are unaffected in *ari-1* mutants (Figure S3G). The observed changes in both Msp-300 localization and Koi levels in *ari-1* mutants provide strong evidence that Ari-1 regulates the LINC complex to control nuclear positioning.

To test if Ari-1 interacts with one of the members of the LINC complex, we performed co-immunoprecipitation (co-IP) experiments in *Drosophila* S2-cells. We found that Ari-1 forms a complex with Koi (Figure 3D and S3H) but fails to interact with other tested LINC components or microtubule-associated proteins (Msp-300, Klar and Ensconsin) (Figure S3H).

We next tested whether the E2 conjugating enzyme (UbcD10) associated with Ari-1 also plays a role in controlling nuclear positioning. First, we confirmed that Ari-1 indeed forms a complex with UbcD10 using S2 cells (Figure S4A). Second, analyses of *ubcD10* mutant (*ubcD10*^{NP2336}) muscles revealed that loss of *ubcD10* causes myonuclear mispositioning and up to 70% of *ubcD10* mutant muscles contain contacting nuclei (Figure 3E). Third, Msp-300 is similarly mislocalized in *ubcD10* mutants as in *ari-1* mutants (Figure 3A and S4B). These data indicate that the same processes are affected in both mutants and that *ari-1*'s control on the position of the nuclei is likely to be ubiquitination-dependent.

Since Koi is upregulated in *ari-1* mutants, it is possible that Ari-1 controls Koi protein turnover through ubiquitination. To assess whether increased levels of Koi impair nuclear anchoring, we expressed Koi-V5 in muscles of wild type flies (C57>Koi-V5). Increasing levels of Koi in muscles phenocopies *ari-1* mutants in many aspects, including 1. nuclear positioning defects in around 60% of the muscles (Figure 3F), 2. Mislocalization of the fraction of Msp-300 that is nuclear-envelope bound (Figure S4C), 3. presence of lamin punctae on the nuclear envelope (Figure S4C), 4. microtubule detachment from the nuclear envelope (Figure S4D), and 5. partial lethality. However, Koi expression leads to a subtle increase in nuclear area (Figure S4E).

To determine if Ari-1 directly ubiquitinates Koi, we first tested if modifying Ari-1 protein levels leads to changes in the ubiquitination status of Koi *in vivo*. However, we were not able to detect ubiquitinated Koi in third instar larvae. In fact, assays to detect endogenous ubiquitination substrates of Ari-1 and its close homolog, Parkin, have not been documented, suggesting that identifying substrates for these E3 ligases *in vivo* is challenging. We therefore performed *in vitro* ubiquitination assays to determine if Koi is a direct target of Ari-1. We first assessed potential ubiquitination sites in the primary amino acid sequence of Koi using UbPred (Radivojac et al. 2010). Potential ubiquitination sites are mostly confined to a 41 kDa domain of the protein (KoiU2, Figure S3E), which we tagged with T7. Under normal conditions, Ari-1's auto-inhibitory Ariadne domain folds to interact with the RING2 domain, preventing the catalytic cysteine that is present in this domain from receiving a ubiquitin molecule and becoming activated (Radivojac et al. 2010, Duda et al., 2013). To relieve auto-inhibition, we pursued two different strategies. First, we purified the Ring1-IBR-Ring2 domains (RBR) of human ARIH1 (Wenzel et al., 2011), which lacks the Ariadne-domain and is enzymatically active. Second, we generated an OPEN mutant of *Drosophila* Ari-1, which contains three missense mutations (F377A, E378A and E450A) that relieve auto-inhibition (Scott et al., 2016, Duda et al., 2013). Finally, to ensure that ubiquitination detected with the OPEN mutant is specific to the function of Ari-1, we generated a third construct that is OPEN-but-catalytically-dead (DEAD). This construct contains the three mutations that are present in the OPEN mutant and a fourth one (C304S) that alters the catalytic cysteine to a serine. All Ari-1 constructs were tagged with GST. We

find that WT, OPEN, as well as the RBR Ari-1 proteins are able to self-ubiquitinate, although the WT protein can self-ubiquitinate to a lesser extent than the OPEN and RBR proteins (Ari-1-Ub(n) and RBR-Ub(n) in Figure 3G). The DEAD Ari-1 protein, in contrast, has no self-ubiquitination activity (Figure 3G, Ari-1 and ubiquitin blots, upper two panels). When blotting for Koi, we observed the unmodified 41 kDa Koi fragment in all reactions to which it was added, but detected an additional higher molecular weight band (~50kDa, KoiU2-Ub) in the reactions catalyzed by the OPEN mutant and, to a lesser extent, the RBR fragment (Figure 3G: KoiU2 blot, bottom). This additional KoiU2 band was also detected when probed for ubiquitin (Figure 3G, Ubiquitin blot, middle panel). The ~50kDa band is not present when the reactions are catalyzed by WT or DEAD Ari-1, or when the reaction lacks ATP or E3 ligase (Figure 3G, ubiquitin blot). To confirm that the 50kDa band is indeed mono-ubiquitinated Koi, we performed both the DEAD and OPEN reactions, subsequently immunoprecipitated Koi and blotted for ubiquitin. We were only able to detect ubiquitinated protein in the OPEN reaction, but not in the DEAD reaction (Figure S4F). These data show that Ari-1 ubiquitinates Koi, and the presence of a single Koi band migrating 8kDa above the full length protein suggests that the modification corresponds to a mono-ubiquitination event.

To confirm that *ari-1* missense mutant alleles, generated in our screen, encode non-functional proteins, we compared the ubiquitination activity of the OPEN allele and the mutant A and B alleles. We introduced the mutations found in each allele into the OPEN construct to generate $OPEN^{A}$ and $OPEN^{B}$, to avoid the auto-inhibition activity of the full length protein. Neither mutant protein is able to ubiquitinate Koi, unlike the wildtype counterpart (s). Hence, the mutant alleles identified from our screen produce inactive E3 ligases.

Does Ari-1 regulate Koi protein turnover? To this end, we performed a cycloheximide pulse chase experiment in S2 cells to determine Koi's turnover in the presence/absence of Ari-1. When inhibiting protein synthesis using cycloheximide, Koi protein levels steadily diminish over time (Right top blot, Figure S4H). This reduction is delayed upon addition of the proteasome inhibitor MG132, indicating that Koi is degraded by the proteasome (Right top blot, Figure S4H). Moreover, reducing endogenous *ari-1* expression using two independent dsRNA shown to be effective in knocking down Ari-1 (left blot, Figure S4H), slows down Koi's turnover (Right bottom blot, s). This indicates that *ari-1* regulates the degradation of Koi.

Ari-1 and Parkin are functionally redundant and missense mutations in Ari-1 affect Parkin

Our observation that complete loss of *ari-1* induces milder phenotypes than missense mutations for all phenotypes tested suggests that other proteins form a complex with Ari-1. The missense mutations in Ari-1 may inhibit the function of a partner(s) with similar functions, causing a more severe phenotype than *ari-1* null mutants. *ari-1* encodes one of five RBR E3-ligases in *Drosophila* (Figure 4A). Ari-1 and CG12362 are the closest paralogs, but expression of the latter protein is restricted to testes (Chintapalli et al., 2007). Moreover, three of the five ligases (Ari-1, Ari-2 and Parkin) are activated by the same E2 enzyme, UbcD10 (Wenzel et al., 2011, Parelkar et al., 2012). Given that (1) Parkin and Ari-1 have

been shown to share interacting partners in mammalian cell lines and (2) both proteins are found in the Lewy Bodies of cases of Parkinson's Disease (Parelkar et al., 2012), both proteins may interact under certain conditions.

To explore if Parkin and Ari-1 interact, we expressed tagged Parkin and Ari-1 in *Drosophila* S2 cells and performed co-IP experiments. As shown in Figure 4B, Ari-1 and Parkin form a complex and the missense mutations of Ari-1 have a greater affinity for Parkin than their wildtype counterpart (Figure 4C and S5A), while Ari-1 mutant proteins have similar or lower affinity for Koi or UbcD10 respectively (Figure S5B). To assess if Ari-1 and Parkin may affect the same pathway, we created double homozygous mutants and tested whether the observed phenotypes are enhanced. *ari-1* mutant animals are pupal lethal with a few adult escapers (Figure 1C) whereas loss of *parkin* ($park^{\Delta 21}$/ $park^{13}$) is homozygous viable and reduces lifespan (Figure 4D)(Pesah et al., 2004, Greene et al., 2003). In contrast, double mutants for *ari-1* and *park* ($ari\text{-}1^{A}$; $park^{\Delta 21}$, $ari\text{-}1^{B}$;$park^{F01590}$, $ari\text{-}1^{D}$;$park^{13}$, $ari\text{-}1^{CRi\{MIC\}}$;$park^{13}$) die as first instar larvae (Figure 4D), suggesting that Parkin and Ari-1 double mutant phenotypes are the result of a synergistic or additive interaction.

If the interaction is synergistic, Parkin should also play a role in myonuclear positioning and its loss, similar to the loss of Ari-1, may affect nuclear shape and positioning. Indeed, laminC staining of $park^{\Delta 21}/park^{F01590}$ mutant muscles revealed that the nuclear envelope of myonuclei is uneven, similar to *ari-1* mutants (Figure 2A and 4E). In addition, 20% of *parkin* null mutant muscles exhibit contacting nuclei, a phenotype that is very rarely observed in wildtype muscles (Figure 4F). These data suggest that Parkin and Ari-1 may indeed have some functional redundancy.

To explore the relationship between the two genes, we performed dominant genetic interaction experiments. Single heterozygous *park* or *ari-1* mutants display clustering defects in 10 and 20% of the muscles respectively (Figure 4F). In contrast, 60% of double heterozygous mutant muscles ($ari\text{-}1^{A}$/+, $park^{21}$/+) display contacting nuclei (Figure 4F). Similar genetic interactions were observed for nuclear morphology. The nuclear envelope in *ari-1* heterozygous ($ari\text{-}1^{A}$/+) muscles show a mild nuclear envelope defect, whereas *parkin* heterozygous ($park^{21}$/+) nuclei are circular (Figure 4E). Again, double heterozygous animals display a much more severe phenotype (Figure 4E). Removal of one copy of *park* in a hemizygous *ari-1* mutant strongly enhances the nuclear morphology defect (Figure 4E). These data strongly support a non-additive role for both Ari-1 and Parkin in nuclear positioning, suggesting that they are partially redundant.

If both proteins are redundant, overexpression of Parkin in *ari-1* mutants should ameliorate observed phenotypes. Indeed, both the nuclear clustering phenotype (Figure 5A) and lethality associated with *ari-1* mutants (Figure 5B) are significantly suppressed. Note that, although we find that Ari-2 can form a complex with both Ari-1 and Parkin (Figure S5E–F), overexpressing Ari-2 does not suppress the nuclear clustering phenotype in an *ari-1* mutant background, showing that the suppression is specific to Parkin (Figure 5A). In summary, these findings show that Parkin can perform some of Ari-1's functions and that the two proteins are functionally redundant in nuclear positioning and morphology.

To address whether the functional redundancy between Ari-1 and Parkin is reciprocal, we determined if over-expressing *ari-1* in a *park* mutant background suppresses *park*-related phenotypes. Parkin regulates mitochondrial health and turnover. In *Drosophila*, loss of *parkin* results in a shortened lifespan and bloated mitochondria in larval muscles (Pesah et al., 2004, Greene et al., 2003, Vos et al., 2012). We first examined mitochondrial morphology by staining the muscles for ATP5A, a component of Complex V. In *parkin* mutants, mitochondria are larger and more globular compared to the mitochondrial network in wild type controls (Figure 5C). Overexpressing human ARIH1 in *parkin* mutants suppresses the mitochondrial morphology phenotype, resulting in smaller mitochondria (Figure 5C). Next, we assessed whether expressing *ARIH1* has an effect on the lifespan of *parkin* mutants. Over-expressing *ARIH1* is able to extend the lifespan of the short-lived *parkin* mutants by 15–50% depending on the genetic background (Figure 5D). Hence, both proteins are functionally redundant. However, Ari-1 probably plays only a minor role in maintaining mitochondrial function, given that *ari-1* mutants do not phenocopy *parkin* mutants and display normal mitochondrial morphology in both adult mutant escapers and larval muscles, although the distribution of mitochondria in the latter is somewhat affected (Figure S6A and B)(Pesah et al., 2004, Greene et al., 2003). The observation that, in contrast to what we observed in the context of nuclear positioning, *ari-1* and *parkin* do not show a dominant genetic interaction in the context of mitochondrial morphology (Figure S6B), suggests that both proteins not only have similar substrates, but have also acquired specific functions that can still be covered when the proteins are overexpressed.

To assess if Parkin can function similarly to Ari-1, we performed co-immunoprecipitation assays and found that Parkin interacts with Koi (Figure 5E). Importantly, when performing *in vitro* ubiquitination assays, we found that Parkin can also mono-ubiquitinate Koi (Figure 5F). Active, self-ubiquitinated Parkin (Park2 RBR Ub(n) in ubiquitin blot), is able to induce a similar 8kDa shift in Koi-U2 (indicated at Figure 5F, T7 blot – arrowhead, ubiquitin blot - *) as we observed for activated Ari-1 (Figure 3G). This finding, together with Parkin's and Ari-1's ability to reciprocally rescue each other's mutant phenotypes (Figure 5A–E), provide compelling evidence that both Ari-1 and Parkin are, to some extent, redundant.

Loss of *ARIH1* in human is associated with thoracic aortic and cerebrovascular disease

Given the pleiotropic phenotypes in *Drosophila ari-1* mutants, we sought to study whether variation in the *ARIH1* gene in humans could cause disease. We noted that *ARIH1* is relatively invariant in individuals that are selected against having Mendelian phenotypes (ExAC database http://exac.broadinstitute.org/gene/ENSG00000166233; MARRVEL.org (Lek et al., 2016, Wang et al., 2017) The probability of loss of function intolerance (pLI score) is 1.00, indicating that *ARIH1* variants may be associated with a dominant disease. These data suggested the possibility that *ARIH1* loss of function alleles may be associated with a Mendelian phenotype and we therefore posted the gene on GeneMatcher (https://genematcher.org)(Sobreira et al., 2015) which led to the discovery of three patients with variants in ARIH1.

Exome sequencing of a cohort of patients with early onset or familial thoracic aortic aneurysm or dissection identified 3 unrelated individuals with rare variants in *ARIH1*. A *de*

novo ARIH1 variant, c.511C>T, p.Arg171Ter (R171*) was identified in case 1 (Figure 6A–B and F). Case 1 is a 17 year old European American (EA) male, originally diagnosed at the age of 6 with fusiform aneurysm of the aortic root and ascending aorta measuring 4.7cm and requiring surgical composite graft repair (Figure 6C). He subsequently developed progressive arch and descending thoracic aortic enlargement that ultimately led to an acute type B dissection and multiple surgical repairs of the aortic arch, descending and thoracoabdominal aorta. Cerebrovascular imaging also showed dilatation of the origin of the brachiocephalic artery and left proximal common carotid artery. He has chronic knee and heel pain that required multiple orthopedic procedures. He has atrophic scars, joint laxity, and pes planus with medial displacement of the malleolus (Figure 6C). Neurologic examination for possible peripheral neuropathy or myopathy was unremarkable. Both his parents are healthy, and his father, brother and paternal half-brother have normal thoracic aortic imaging (Figure 6A–B). His maternal half-sister died at 2 years of age from myocarditis by report; her medical records are not available (Figure 6A–B).

Exome sequencing of 220 affected probands from families with two or more members with thoracic aortic disease identified two additional probands with *ARIH1* variants (case 2 and case 3, Figure 6A, D–F). Case 2, a 72 year old EA woman with basilar tip artery aneurysm and distal left internal carotid artery aneurysm but a normal aorta, has an *ARIH1* c.131A>G, p.Glu44Gly (E44G, Figure 6A, D and F) variant. Her brother, paternal uncle and paternal first cousin also had intracranial aneurysms (Figure 6A and D). Her father had surgical repair of a thoracic aortic aneurysm in his late 40s (Figure 6A and D). Her sister was diagnosed with a thoracic aortic aneurysm and underwent repair at the age of 70 years (Figure 6A and D). DNA samples were not available from affected relatives to confirm segregation of the variant with vascular disease.

Case 3 has an *ARIH1* c.43G>C, p.Glu15Gln variant (E15Q, Figure 6A, E–F) and is a 55 year old EA woman who presented at the age of 52 years with an acute type A aortic dissection and 5.1 cm ascending aortic aneurysm. Her 57-year-old brother who has ascending aortic aneurysm also carries the *ARIH1* variant. Their mother and brother died suddenly of unidentified causes but possibly due to dissections at the age of 59 and 52 years, respectively, but DNA samples were not available (Figure 6A, E).

To examine if the identified human variants impair ARIH1 function, we turned to *Drosophila*. We introduced the identified mutations (R171*, E15Q and E44G) in human *ARIH1* cDNA and ubiquitously expressed them. We showed that expression levels of wildtype ARIH1 and mutant proteins, E15Q and E44G are very similar (Figure S7A). R171* cannot be detected because the epitope of the antibody is not present. To test if mutations in ARIH1 produce functional proteins, we ubiquitously expressed the different ARIH1 variants in *ari-1* mutants and showed that all human mutations fail to rescue nuclear positioning and lethality (Figure 6G and 7A). In addition, escapers expressing the mutant forms of *ARIH1* survive only a few days (Figure 6H). Hence, the three human *ARIH1* variants result in loss of function of ARIH1.

To determine if the identified rare *ARIH1* variants induced nuclear morphology defects, we examined the ultrastructure of the patients' aortic tissues using TEM. In contrast to syncytial

skeletal muscles, determining the precise position of nuclei in mononucleated vSMCs is challenging. We therefore compared nuclear morphology of aortic vSMCs obtained from healthy individuals to patient samples. The nuclear envelope in healthy vSMCs is generally smooth and round. However, in patient Case 1 and Case 3, the nuclear envelope is irregular and contains numerous folds and indentations (Figure 7B). Patient samples have a significantly reduced ratio of nuclear area to circumference when compared to controls (Figure 7B), indicating that the nuclear envelope in the patient samples are indeed irregular because of an increase in folds. The nuclear morphological changes observed in patients' vSMCs are likely attributable to loss of *ARIH1*, as reducing ARIH1-levels by 50–80% using three independent shRNA constructs (Figure S7B–C) causes a significant decrease in the percentage of nuclei with normal morphology compared to scrambled shRNA control (Figure 7C). In addition, these cells display defects in the microtubule network, whereas mitochondrial morphology is unaffected (Figure S7D and E). Finally, we tested the protein levels of Koi homologs SUN1 and SUN2. *ARIH1* knockdown leads to a 50–60% increase in SUN2 levels, whereas SUN1 remains unchanged (Figure S7C). The increase in SUN2 protein level is a post-transcriptional event, since SUN2 transcripts are reduced upon *ARIH1* knock down (Figure S7F).

Discussion

Our study reveals that the RBR E3 ubiquitin ligase Ari-1 regulates the subcellular localization and morphology of muscle nuclei in flies. Loss of *ari-1* affects the protein levels and/or distribution of members of the LINC complex. Interestingly, Ari-1 and Parkin, a second RBR E3 ligase family member, exhibit redundant functions. Indeed, overexpressing *parkin* in *ari-1* mutants suppresses the observed phenotypes and vice versa (Figure 5). We show that Koi, a subunit of the LINC complex can be ubiquitinated by both Ari-1 and Parkin (Figure 3G and 5F). Finally, we identify rare dominant variants in the human homolog of *ari-1*, *ARIH1*. These variants are associated with cerebrovascular and aortic aneurysms and we document that patient samples have altered nuclear morphology (Figure 6 and 7).

How does Ari-1 regulate the placement and shape of nuclei?

Loss of *ari-1* leads to clustering of nuclei in *Drosophila* striatal skeletal muscles (Figure 1D–E). We find that the protein distribution of several LINC complex members is affected in *ari-1* mutants (Figure 2A, 3A–B). Our data show that Koi is the target of Ari-1. First, Koi protein levels are upregulated in *ari-1* mutants, whereas Koi mRNA levels remain unchanged (Figure 3B–C; S3G). Second, in human vSMCs, the protein level of the Koi homolog, SUN2, is elevated upon *ARIH1* knockdown (Figure S7C). Third, over-expressing Koi phenocopies *ari-1* mutants (Figure 3F, S4C–D). Fourth, Koi is the only LINC complex member that physically interacts with Ari-1 when tested in cell culture (Figure 3D and S3H). Fifth, Ari-1 mono-ubiquitinates Koi in *in vitro* experiments (Figure 3G and S4F). We propose that Ari-1's mono-ubiquitination of Koi primes Koi for subsequent poly-ubiquitination and degradation by another E3 ligase. This other E3 ligase could be Cullin-1, as in human cells, the Cullin-1 ubiquitination complex regulates the turnover of SUN2 (Coyaud et al., 2015). Furthermore, a cooperative ubiquitin-tagging activity has been shown for vertebrate ARIH1 and Cullin-1 (Scott et al., 2016).

How do elevated levels of Koi impair the LINC complex? One possibility is that excessive amounts of Koi proteins disrupt the stoichiometry of the functional LINC complex, resulting in imbalanced mechanical tensions applied across the nuclear envelope. Also, excessive Koi at the nuclear envelope may redistribute Koi to other compartments continuous to the nuclear envelope, including the ER. In fact, over-expressed SUN1 was found to enter the ER-Golgi secretory pathway, and retention of SUN in the Golgi is associated with the pathology of laminopathies (Chen et al., 2012), supporting our observations that elevated Koi/SUN levels can lead to cellular and physiological defects.

Ari-1 missense mutations act as recessive antimorphs

The observation that a missense mutation induces a stronger phenotype than its corresponding null mutation was recently dubbed “recessive antimorph” (Sijacic et al., 2011). This genetic phenomenon reveals the presence of a second, functionally redundant protein that is inhibited by a missense mutant, but can execute its function in the absence of the protein. Our data suggest that the missense mutations function as recessive antimorphs because 1) the mutations cause recessive lethality with a dominant muscle nuclear phenotype (Figure 1C and E); 2) mutant phenotypes are rescued by introducing wild type copies of the gene (Figure 1C and E); 3) Crossing *ari-1* missense mutant alleles to a deficiency diminishes the nuclear positioning phenotype compared to homozygous/hemizygous missense mutants (Figure 1E) and 4) The missense mutant alleles can be rescued in a dose-dependent fashion (Figure 1E). These findings strongly support the view that the three identified missense mutations behave as dominant negative alleles.

Ari-1 and Parkin are partially redundant

Ari-1 and Parkin are members of the same E3 ligase subfamily and are evolutionarily related. An evolutionary tree of the RBR-domains of all Ariadne and Parkin RBR proteins, reveals that *ariadne* gene are the ancestral genes as they – in contrast to *parkin* – are present in all unicellular eukaryotic organisms tested (Eisenhaber et al., 2007). Parkin has an established role in mitochondrial quality control (Haelterman et al., 2014b). However, loss of *PARK2* homologs have been associated with significant phenotypic discrepancies across species and even among cell types in the same organism (Pesah et al., 2004, Greene et al., 2003, Palacino et al., 2004, Goldberg et al., 2003, Von Coelln et al., 2004). These differences have challenged our ability to unravel the *in vivo* role of Parkin, and have questioned the cellular requirements of Parkin. Our data argue that there is some functional redundancy between Ari-1 and Parkin. First, the double homozygous mutants are first instar lethal whereas the single null mutants are viable (*parkin*) or late pupal lethal with escapers (*ari-1*) (Figure 4D). Second, double heterozygous mutants display a much stronger myonuclear clustering phenotype than either heterozygous mutant (Figure 4F). Third, overexpressing Parkin partially rescues *ari-1* mutant phenotypes (Figure 5A–B). Fourth, overexpressing *ARIH1* in *parkin* mutants ameliorates phenotypes associated with the loss of *parkin* (Figure 5C–D). Moreover, Ari-1 and Parkin can form homodimers or homomultimers (Figure S5C–D). In addition, Ari-1 can be found in a complex with Parkin (Figure 4B). Our data are therefore most consistent with the following model (Figure 7D): we propose that there are three complexes: Ari-1/Ari-1; Parkin/Parkin; Ari-1/Parkin, each of which can perform some functions related to nuclear and mitochondrial phenotypes but they differ in efficiency.

Under normal conditions, Ari-1 mainly regulates nuclear positioning and morphology but is aided by Parkin (Figure 7D left panel). In the absence of Ari-1, Parkin can still regulate nuclear positioning, but with lower efficiency leading to a mild nuclear clustering phenotype (Figure 7D middle panel). Although the requirement of Ari-1 is clearly more prominent for nuclear phenotypes than the requirement of Parkin, the reverse is true for mitochondrial quality control. In the latter case, Parkin plays the major role and no mitochondrial morphology phenotype is observed in Ari-1 mutants; but Ari-1 can clearly suppress some of the mitochondrial phenotypes associated with loss of *parkin* (Figure S6B and 5C). Finally, in an *ari-1* missense mutant background, mutant Ari-1 sequesters Parkin in a non-functional complex, causing a stronger nuclear positioning phenotype (Figure 7D right panel).

Is this functional redundancy observed among all RBR family members? Although our data show that Ari-1, Parkin and Ari-2 can form pairwise complexes such as Ari-1/Ari-2; Parkin/Ari-1; Parkin/Ari-2 (Figure S5E–F), over-expressing Ari-2 does not rescue nuclear clustering phenotypes in *ari-1* mutants (Figure 5A), suggesting no redundancy exists between these two Ari members for this function. It is, however, possible that in different cellular contexts, one or more RBR protein(s) may be able to compensate for the loss of another RBR protein, and different species may have evolved to express these proteins at different levels in various tissues. Hence, the observed phenotypic discrepancies between *parkin* mutants in different species and cells may be attributable to redundancy/dependency issues between the Ari-1 and Parkin isoforms.

Mutations in *ARIH1* are associated with aortic aneurysm and dissection

We identified three rare variants in *ARIH1* in patients with aortic and cerebrovascular aneurysm (Figure 6A–F). All three variants likely represent loss-of-function alleles because they, in contrast to wildtype *ARIH1*, fail to rescue nuclear clustering, eclosion, and longevity of *ari-1* mutant flies (Figure 6G–H, 7A). Similarly, the nuclei of patients' vSMCs display aberrant nuclear morphology (Figure 7B), and reducing *ARIH1* expression in vSMCs induces nuclear morphological changes as observed in the patients (Figure 7C).

How could loss of *ARIH1* lead to aneurysms? To date, the genes associated with aortic aneurysms can be divided into several groups based on the cellular process that are affected, one of which is cellular mechanotransduction. Mechanotransduction is important for muscles to adapt and respond to dynamic mechanical forces in their environment (Volk and Wang, 2015). In SMCs, proper contraction and mechanosensing depends on functional contractile units and their connections to the extracellular matrix through focal adhesions. Genes that encode major structural components of the contractile unit, *ACTA2* (encodes SMC-specific α-actin) (Guo et al., 2007), *MYH11* (SMC-specific myosin heavy chain) (Khau Van Kien et al., 2005), *MYLK* (myosin light chain kinase) (Wang et al., 2010),*PRKG1* (type I cGMP-dependent protein kinase) (Guo et al., 2013) and the extracellular matrix component, *FBN1* (encodes fibrillin-1) have shown to be mutated in aortic aneurysm patients. It has been proposed that in these cases, mechanotransduction between vSMCs and the extracellular matrix (ECM) is impaired, affecting mechanosensing of the vSMCs and hereby altering molecular pathways leading to aortic disease (Milewicz et al., 2016). Given that contractile units in vSMCs are connected to both the focal adhesions

and the nuclear membrane, and that proper mechanosensing is important in preventing aneurysms, the observation that *ARIH1* disease-associated variants disrupt the nuclear envelope's structure in vSMCs implicates a defect in mechanosensing that may be responsible for the aortic and cereobrovascular diseases.

Interestingly, a growing body of evidence implicates the LINC complex in mechanosensing (Neelam et al., 2015, Guilluy and Burridge, 2015). Integrin adhesion complexes relay extracellular signals via the cytoskeleton and the LINC complex onto the nuclear envelope to permit mechano-regulation of gene expression (Alam et al., 2016). Mutations in the LINC complex members have been associated with striatal and cardiac muscle diseases as well as vascular diseases. For example, mutations in Lamin (*LMNA*), and SUN genes (*SUN1* and *2*) are associated with muscular dystrophies (Meinke et al., 2014, Bonne et al., 1999). Interestingly, missense mutations in SYNE1 (the human Msp-300 homolog) are associated with a dominant muscular dystrophies, while mutations that encode truncated SYNE1 cause recessive cerebellar ataxias with no overt muscular phenotype (Zhang et al., 2007, Gros-Louis et al., 2007). However, all of the above mutations affect nuclear positioning or nuclear envelope integrity.

Given that Ari-1 regulates the LINC complex in flies, it is highly likely that it assumes a similar role in human vSMCs. Loss of *ARIH1* in aortic vSMCs would hereby affect mechanosensing, weaken the aortic wall muscles to induce aneurysms and dissections. It is intriguing to note that patients with *ARIH1* mutations have no reported skeletal muscle abnormalities, even though mutations in members of the LINC complex are associated with muscular dystrophies (Zhang et al., 2007, Meinke et al., 2014, Bonne et al., 1999). Our data suggest that functional redundancies of RBR proteins in skeletal muscles may underlie the lack of phenotype. Interestingly, patients with Parkinson's Disease are about two times more likely to develop heart failure (Zesiewicz et al., 2004), suggesting that *parkin* may be a risk factor for heart disease.

In summary, Ari-1 regulates nuclear morphology in *Drosophila* skeletal muscles and human vSMCs. Loss of *ARIH1* is associated with aortic and cerebrovascular aneurysms, likely due to the disruption of mechanosensing in vSMCs. We also find that Ari-1 and Parkin are to some extent functionally redundant as either gene can partially suppress some of the phenotypes associated with the loss of the other gene. Hence, Ari-1 and Parkin regulate nuclear positioning and mitochondrial quality control respectively but have each retained the ability to perform both functions to some extent.

STAR Methods

EXPERIMENTAL MODEL AND SUBJECT DETAILS

Patient details—IRB approval and informed consent were obtained from the human subjects with *ARIH1* variants.

Case 1: Case 1 is a 17 year old European American (EA) male, originally diagnosed at the age of 6 with fusiform aneurysm of the aortic root and ascending aorta measuring 4.7cm and requiring surgical composite graft repair (Figure 6C). He subsequently developed

progressive arch and descending thoracic aortic enlargement that ultimately led to an acute type B dissection and multiple surgical repairs of the aortic arch, descending and thoracoabdominal aorta. Cerebrovascular imaging also showed dilatation of the origin of the brachiocephalic artery and left proximal common carotid artery. He has chronic knee and heel pain that required multiple orthopedic procedures. He has atrophic scars, joint laxity, and pes planus with medial displacement of the malleolus (Figure 6C). Neurologic examination for possible peripheral neuropathy or myopathy was unremarkable. Both his parents are healthy, and his father, brother and paternal half-brother have normal thoracic aortic imaging (Figure 6A–B). His maternal half-sister died at 2 years of age from myocarditis by report; her medical records are not available (Figure 6A–B).

Case 2: Case 2, a 72 year old EA woman with basilar tip artery aneurysm and distal left internal carotid artery aneurysm but a normal aorta, has an *ARIH1* c.131A>G, p.Glu44Gly (E44G, Figure 6A, D and F) variant. Her brother, paternal uncle and paternal first cousin also had intracranial aneurysms (Figure 6A and D). Her father had surgical repair of a thoracic aortic aneurysm in his late 40s (Figure 6A and D). Her sister was diagnosed with a thoracic aortic aneurysm and underwent repair at the age of 70 years (Figure 6A and D). DNA samples were not available from affected relatives to confirm segregation of the variant with vascular disease.

Case 3: Case 3 has an *ARIH1* c.43G>C, p.Glu15Gln variant (E15Q, Figure 6A, E–F) and is a 55 year old EA woman who presented at the age of 52 years with an acute type A aortic dissection and 5.1 cm ascending aortic aneurysm. Her 57-year-old brother who has ascending aortic aneurysm also carries the *ARIH1* variant. Their mother and brother died suddenly of unidentified causes but possibly due to dissections at the age of 59 and 52 years, respectively, but DNA samples were not available (Figure 6A, E).

Fly Stocks and Genetics—Mutant *ari-1* alleles ($ari\text{-}1^{A}$, $ari\text{-}1^{B}$ and $ari\text{-}1^{D}$) were generated in a previously described mutagenesis screen (Haelterman et al., 2014a, Yamamoto et al., 2014). These alleles were balanced with FM7c Kr> GFP (Yamamoto et al., 2014). Hemizygous mutant animals were separated from their wildtype siblings by selecting against GFP. The generation of $ari\text{-}1^{CRI\{MIC\}}$, $ari\text{-}1^{GFSTF}$ and $ari\text{-}1^{T2A\text{-}Gal4}$ is detailed in the following section. Control lines used are *FRT,P{neoFRT}19A iso* and $y^{1}w^{*}$ *and w*, P{GawB}C57 (C57-GAL4)* (FBti0016293) (Brand and Perrimon, 1993). For genomic rescue experiments, $Df(1)os^{UE69}/C(1)DX, y^{1}\ f^{1}/Dp(1;Y)W39, y^{+}$ (dp1538, FBab0003184), as well as w^{1118}*; Dp(1;3)DC342, PBac{DC342}VK00033* (80 kb P, FBab0046572) (Venken et al., 2010) were used. In most experiments, males of *ari-1** and *ari-1*;GR* were used, except when female *ari-1* mutants carrying two different alleles of *ari-1* shown, for example $ari\text{-}1^{A/B}$, $ari\text{-}1^{A/+}$ or $ari\text{-}1^{A/def}$. GR indicates two exogenous copies of wildtype *ari-1* genomic region. cDNA rescue experiments: $y\ w\ ;\ P[(w^{+})\ UAS\text{-}ari\text{-}1^{+}$ and *y w ; P[(w+)UAS-ARIH1] / CyO* are gifts from Dr. Alberto Ferrus(Gradilla et al., 2011). GAL4 lines: *P{Gal4-da.G32}* UH1 (ubiquitous, FBti001399), P{GAL4-Mef2.R}3 (muscle, FBti0115746). Deficiency (def) lines: $Df(1)BSC352, w^{1118}/FM7h/Dp(2;Y)G, P\{hs\text{-}hid\}Y$ (*ari-1*, FBst0024376), w^{1118}*; Df(2R)Exel6050, P{XP-U}Exel6050/CyO* (*koi*, FBst0007532), w^{1118}*; Df(2R)BSC347/CyO* (*ubcD10*, FBst0024371). Mutant lines: *w*;*

P{GawB}Ubc10^{NP2336} / CyO (FBst0303027), *w^{1118}; P{GT1}Ubc10^{BG00902}/CyO* (FBst0012444). *koi^{84}* was a gift from Janice Fischer(Kracklauer et al., 2007). *park$^{\Delta 21}$* and *park^{13}* are null alleles of *parkin* that were independently generated by P-element imprecise excision(Pesah et al., 2004, Greene et al., 2003). *PBac{WH}parkf01950 (park^{f01950})* is a PiggyBac insertion in the second exon of *parkin* (Thibault et al., 2004). For ERG experiments, homozygous mutant eye clones were generated by crossing *ari-1* P{neoFRT}19A/FM7c* females to *FRTcl(1),P{neoFRT}19A/Dp(1;Y),y^{+},v^{+}; ey-FLP* males (Newsome et al., 2000). Fly lines containing pUAST-attB-ARIH1 variants (VK37), pUASTattB-Koi-V5 (VK37) and pUASTattB-Ari-2-V5 (VK37) were generated in this study (detailed in Methods: plasmid constructs and cloning).

***ari-1* CRI{MIC}, *ari-1* CRI{GFSTF} and *ari-1* CRI{T2A-Gal4}:** *ari-1* CRI{MIC}, *ari-1* CRI{GFSTF} and *ari-1* CRI{T2A-Gal4} were generated in this study (detailed in Methods: Generation of *ari-1* gene traps and protein trap).

Cell lines (oligonucleotides used are detailed in Supplementary Table)

***Drosophila* S2 cells:** S2 cells were cultured at 25°C in Schneider's medium (Life Technologies) plus 10% heat-inactivated fetal bovine serum (Sigma, #F4135), 100 U/mL penicillin (Life Technologies), and 100 μg/mL streptomycin (Life Technologies). Cells were split every 3 days and plated at a density of 2×10^6/flask in 25cm^2 cell culture flasks (Fisher Scientific) for experiments. Transfections were carried out using Effectene transfection reagent following standard procedures (Qiagen, # 301425). Expression of genes in pUASTattB constructs were performed by co-transfecting of Actin-GAL4-containing plasmid. For negative controls, empty pUASTattB vectors are co-transfected with gene-containing pUASTattB constructs (as stated in figures) to maintain equal GAL4 activation as in experimental studies. For expression of genes in pMK33 constructs, cells were induced with 0.7mM $CuSO_4$ 24 hours post-transfection.

Human aortic smooth muscle cells: Approval from the University of Texas Health Science Center at Houston Institutional Review Board to use anonymized donor aortic tissue for research was obtained. Immortalized human aortic smooth muscle cells (vSMCs, MG11023) (Guo et al., 2017) were grown in SmGM-2 complete media (Lonza, #CC-3182) with 20% FBS (Atlanta). For induction of smooth muscle differentiation, cells were serum starved in 1% FBS for 24 hours followed by treatment with TGF-β1 at 2ng/ml (R&D Systems). To knockdown the expression of *ARIH1*, three pzGipz lentiviral shARIH1 constructs as well as a scrambled shRNA (sequence: TCTCGCTTGGGCGAGAGTAAG), were obtained from GE Dharmacon (03: V3LHS_334303, 05: V2LHS_199505, 15: V2LHS_199015) The shRNA constructs were transfected in the HEK293T packaging cell line, together with the packaging plasmids pSPAX2 and pMD2.G using Lipofectamine 3000 (Life Technologies) and incubated for 48 hours in a 37°C incubator. The supernatants containing lentivirus from the transfected packaging cells were filter sterilized using 0.46mm filter (Milipore) and concentrated with LENTI-X concentrator (Clontech) following the manufacturer's instructions. The concentrated lentiviruses were used to infect immortalized human SM cell line 11023 with polybrene at 8μg/ml. 48 hours post-infection, cells were seeded in 6-well

plates for further experiments. The knockdown efficiency of ARIH1 was subsequently analyzed by Western blot.

METHOD DETAILS

Plasmids (oligonucleotides used are detailed in Supplementary Table)—

pMK33-klar-C-FLAG-HA: protein fragment expressed is part of isoform PA (starting amino acid: 1774), isoform PB (starting amino acid: 1556), isoform PE (starting amino acid: 1784), isoform PG (starting amino acid: 692) and isoform PI (starting amino acid: 33). pMK33-Msp300-C-FLAG-HA: protein fragment expressed is part of isoforms PB, PD, PL (starting amino acid: 7976), isoforms PE, PF, PG, PH, PM (starting amino acid: 1) and isoform PL (starting amino acid: 7616). Both pMK33 clones are gifts from Dr. Wade Harper (Guruharsha et al., 2011, Yu et al., 2011). UAS-ensconsin-HA is a gift from Mary Baylies (Metzger et al., 2012). The PGEX-4T-HHARI RBR and PGEX-4T2-Parkin RBR constructs was previously published and was obtained from Addgene (#31254 and #31255)(Wenzel et al., 2011). All oligos used (Sigma) for construct generation (below) are detailed in Supplementary Table 1. PCRs were performed using Q5 2X master mix (NEB).

pUASTattB ari-1: A plasmid containing full length *ari-1* cDNA (plasmid RE69116) was obtained from Berkeley *Drosophila* Genome Project (BDGP) and subcloned into pUASTattB (Bischof et al., 2013) using BglII and XbaI sites (NEB). Two versions (N-terminal V5 and HA tags) were designed in-frame with *ari-1* Different variants of pUASTattB_ari-1 were generated by site-directed mutagenesis using QuikChange XL site-directed mutagenesis Kit (Agilent Technologies) using pUASTattB_ari1 as template.

pUASTattB_parkin: A plasmid containing full length *parkin* cDNA (SD01679) was obtained from BDGP and subcloned into pUASTattB (Bischof et al., 2013) using BglII and XbaI sites (NEB). Two versions (N-terminal Flag and HA tags) were designed in-frame with *parkin*.

pUASTattB_ubcD10: A plasmid containing full length *ubcD10* cDNA (RE47264) was obtained from BDGP and subcloned into an EGFP-containing pUASTattB, designed as such for an insert to be in frame with a C-terminal EGFP tag. The *ubcD10* PCR products and pUASTattB-C-EGFP were digested with KpnI and XbaI (NEB).

pUASTattB_koi: A plasmid containing the N-terminal of *koi* cDNA (koi^{Nterm}, RE12054, covering amino acids 1–441 of PB isoform; Supplementary Fig. 3b) was obtained from BDGP. koi^{Nterm} was subcloned into an EGFP-containing pUASTattB, designed for the insert to be in frame with an N-terminal EGFP tag. The koi^{Nterm} PCR products and pUASTattB-N-EGFP were digested with BglII and XbaI (NEB).

A plasmid containing the C-terminal of *koi* cDNA (koi^{Cterm}, RT06825, covering amino acids 563–967 of PA isoform; Supplementary Fig. 3b) was obtained from BDGP. Two versions (N-terminal V5 and GFP tags) were designed in-frame with koi^{Cterm}. The koi^{Cterm} PCR products (both V5 and GFP tags) and vectors were digested with BglII and XbaI (NEB).

Koi full length (PA isoform) was generated using Gibson Assembly (NEB) by combining three DNA fragments covering the 5′ end (RE12054, BDGP), the 3′ end (RT06825, BDGP) and a 170-base fragment in between that is not covered by either of the clones (synthesized by Integrated DNA Technologies). An N-terminal V5-tag was incorporated via PCR to the assembled full length Koi cDNA, which was subsequently cloned to pUAST-attB. All PCR products and vectors were digested with BglII and XbaI (NEB).

pUASTattb_ARIH1^{variant}: Wild type full length *ARIH1* cDNA was obtained from the Harvard PlasmID Database (clone HsCD00338442) and subcloned into the pUASTattB vector using NotI and XhoI restriction sites (NEB). Variants were subsequently generated using the QuikChange II XL Site-Directed Mutagenesis kit (Agilent Technologies). *ARIH1*-variant-containing pUASTattB was micro-injected into $y^1 w^*$; *VK37* embryos.

pUASTattB_ari-2: Plasmid containing *ari-2* cDNA (GH01766) was obtained from BDGP. Full length *ari-2* cDNA was subcloned into pUASTattB. Two versions (N-terminal V5 and Flag tags) of pUASTattB_ari-2 were generated. The *ari-2* PCR products and pUASTattB were digested with NotI and XbaI (NEB). pUASTattB_ari-2-V5 was subsequently micro-injected into $y^1 w^*$; *VK37* embryos.

PGEX-4T1_ari-1^{variants}: Wild type, full length *ari-1* cDNA was subcloned into PGEX4T-1, in frame with an N-terminal GST tag. Variants of *ari-1* cDNA (DEAD and OPEN) were generated by site-directed mutagenesis using the QuikChange XL site-directed mutagenesis Kit (Agilent Technologies). Mutations introduced to generate the OPEN mutant: F377A, E378A and E450A mutations. For the DEAD mutant we introduced F377A, E378A, E450A and C304S. Mutations introduced to generate OPEN^A mutant: F377A, E378A, E450A and C136Y. Mutations introduced to generate OPEN^B mutant: F377A, E378A, E450A, V187E and S322P.

pET28a_KoiU2: Potential Koi uiquitination sites were predicted using UbPred, an online software generated to predict ubiquitination sites in proteins using random forest (Radivojac et al.). A fragment of Koi cDNA (amino acid 403-776 of A isoform, KoiU2), predicted to contain a group of lysines with high ubiquitination probability, were subcloned into the pET28a vector (Novagen), so that the *koiU2* cDNA is in frame with N-terminal His and T7 tags.

Generation of *ari-1* gene traps and protein trap (oligonucleotides used are detailed in Supplementary Table)—PM15 vector (Supplementary Fig. 2a): the CRI{MIC} vector was synthesized as follows: DNA Fragments “attP-FRT-SA-3×STOP-SV40pA-3XP3” and “shmiR for white-ftz intron-SV40pA-FRT-attP” were commercially synthesized (Life technologies). Fragments were amplified by PCR as BstX1-BsmBI-BsaI-BbsI-attP-FRT-SA-3×STOP-SV40pA-3XP3-EagI and EagI-shmiR white-ftz intron-SV40pA-FRT-attP-BbsI-BsaI-BsmBI-EcoRV and cloned into a modified pBS vector (deleted BsaI) to create PM15.

ari-1 $^{CRI\{MIC\}}$: *ari-1 $^{CRI\{MIC\}}$* was generated using CRISPR/Cas9 technology. DRSC/TRiP functional genomics resources were used to identify the sgRNA site against the first coding

intron of *ari-1* (between the first and second coding exon). Subsequently, DNA sequences encoding the sgRNA oligos (Sigma) were cloned using BbsI into pCFD3:U6:3-gRNA, a gift from Simon Bullock (Addgene plasmid # 49410)(Port et al., 2014). To induce homologous recombination and insert the gene trap cassette at the sgRNA-mediated Cas9 cleavage site, 500 bases upstream and downstream of the cleavage site (a1 and a2) were cloned into PM15 (generated in this study), flanking the gene trap cassette. a1 was cloned using BstI and NsiI restriction sites, whereas a2 was cloned using SphI and XhoI restriction sites. Insertions were confirmed using PCR and sequencing. The modified pCFD3:U6:3-gRNA and PM15 were then co-injected into $y^{-}v^{-}$; {*nos-Cas9* y^{+} v^{+}}/*Cyo* embryos (NIG-FLY). PM15 contains a dominant marker to ease the identification of flies that have incorporated the construct. Mutant flies can be recognized by a loss (or reduced level) of the red pigment in the eye, due to the presence of an shRNA against *white* (*w*) that is specifically expressed in the eye (3×P3 promoter). Injected adults were crossed to CantonS to screen for animals and altered eye color. Single, reduced-red eye females were crossed to *FM7, Kr>GFP/Y* males to generate stable stocks of *ari-1*$^{CRi\{MIC\}}$. The presence of the gene trap in these stocks was confirmed through PCR and Sanger sequencing, using a primer outside of the insert region, and a second primer within the gene trap construct. All primers used are detailed in the Primer table.

ari-1 $^{CRI\{GFSTF\}}$: *ari-1*$^{CRi\{MIC\}}$*/FM7, Kr>GFP* embryos were injected with a multi-tag-containing vector (EGFP-FlAsH-StrepII-3×Flag) and a phiC31-expression vector to allow RMCE at the *ari-1* CRI{MIC} locus (as described in Venken et al., 2011). Injected adult females were crossed to *FM7, Kr>GFP/Y*. Single females were crossed to *FM7c, P{GAL4-Kr.C}DC1, P{UAS-GFP.S65T}DC5, sn*+ to generate stable stocks. Homozygous viable lines containing flies with complete red eye were retained.

ari-1 $^{CRI\{T2A\text{-}Gal4\}}$: The gene trap cassette in the *ari-1*$^{CRi\{MIC\}}$*/FM7, Kr>GFP* flies was replaced with a T2A-Gal4 cassette (lox2-attB2-SA-T2A-Gal4-Hsp70) using phiC31-mediated recombination through genetic crosses (Nagarkar-Jaiswal et al., 2015a). Finally, *ari-1*$^{T2A\text{-}GAL4}$*/FM7c was* kept as stock.

RNA-isolation and RT-qPCR ((oligonucleotides used are detailed in Supplementary Table)—Total RNA was isolated from ten third instar larvae per genotype, following standard procedures. Briefly, animals were flash frozen and subsequently homogenized in 1ml TRIzol (ThermoFisher Scientific, #15596026). Samples were incubated for 5 min, 200 µl Chloroform was added, samples were vortexed and incubated for 5 minutes at room temperature. Next, samples were centrifuged at maximum speed for 5 minutes, 150 µl of the top layer was transferred into a new eppendorf tube, containing 500 µl Isopropanol and incubated for 10 minutes at room temperature. A 20 minute centrifugation step (maximum speed) allowed precipitation of the RNA. The pellet was washed with 70% ethanol and resuspended in 50µl of DEPC-treated water. Five micrograms of total RNA from each sample was reverse transcribed using Random Hexamer Primers and the High-Capacity cDNA Reverse Transcription Kit (Applied Biosystems, # 4368814). Technical and biological triplicates were performed to achieve the mean and error bars presented. Real-time PCR was carried out in a thermal cycler (iCycler; Bio-Rad

Laboratories), using iQ™ SYBR® Green Supermix (Bio-Rad, #1725121). Data was collected and analyzed using the optical module (iQ5; Bio-Rad Laboratories). All primers used are detailed in Primer table.

Cycloheximide pulse chase (oligonucleotides used are detailed in Supplementary Table)—0.2 million cells/well were plated in 12-well plate. 4 hours post-seeding, 9μg of dsRNA was added into each well. 24 hours post-seeding, cells were transfected with Actin-GAL4 and pUASTattB_KoiV5. CHX (100uM, Sigma) and MG132 (50uM, Sigma) in dimethyl sulfoxide (DMSO) were added to S2 cells 48 hours after transfection and incubated for indicated time. Ari-1 and GFP dsRNAs were synthesized with MEGAscript T7 Transcription Kit (Thermo Fisher Scientific). The primers used to generate the dsRNAs are detailed in Primer Table.

Co-immunoprecipitation and western Blot analysis—48 hours after transfection, S2 cells were lysed for 30 minutes on ice, using 1X lysis buffer (Cell Signaling, #9803) with EDTA-free proteinase inhibitor (Thermo Scientific, #88266). The lysates were centrifuged at maximum speed for 10 minutes at 4°C. Next, supernatants were transferred to a clean eppendorf tube and incubated overnight at 4°C with 5 μl agarose beads, which had been previously equilibrated with lysis buffer. The beads were washed 3 times in washing buffer (Tris-HCl 10mM, pH 7.5, NaCl 150mM, EDTA 0.5 mM) before boiling in loading buffer. Western blotting was then performed with each sample. The following beads were used for immunoprecipitation: Chromotek-GFP-Trap Agarose Beads (Allele Biotechnology, # ACT-CM-GFA0050), Monoclonal Anti-V5–Agarose andbody (Sigma, A7345), monoclonal anti-FlagM2-agarose antibody (Sigma, A2220), monoclonal anti-HA-Agarose antibody (Sigma) and monoclonal anti-T7-agarose antibody (EMD Millipore). The antibodies used for Western blot analyses were: rabbit anti-GFP (1/2000 Thermo Fisher, A11122), mouse anti-HA (1/2000, 16B12, Covance), mouse anti-Flag (1/2000, M2) and mouse anti-V5 (1/2000, Thermo Fisher, R960-25), goat anti-GST (1/2000, Amersham), Rabbit anti-T7 (1/5000, Novus Biologicals), Streptavidin-HRP (1/5000), goat anti-ARIH1 (1/1000, ab3891, abcam), rabbit anti-SUN1 (1/1000, ab124770, abcam), rabbit anti-SUN2 (1/1000, ab124916, abcam) mouse anti-GAPDH (1/10,000, 14C10, Cell signaling).

Immunohistochemistry—Third instar larvae were dissected in PBS, fixed for 20 minutes either in methanol (−20°C) or in PBS containing 3.7% formaldehyde (room temperature) and washed in PBS, containing 0.2% Triton X-100 (PBT). Fixed tissues were blocked in PBT, 10% normal goat serum (NGS) for 1h at room temperature and incubated in primary antibodies overnight at 4°C, rocking. Samples were washed in PBT, incubated in secondary antibody diluted in PBT for one hour at room temperature, and washed in PBT prior to mounting. Primary antibodies were used at the following dilutions (in PBT, 10% NGS): mouse anti-laminC (LC28.26, DSHB, (Riemer et al., 1995)): 1/250; Guinea Pig anti-Msp-300 (Elhanany-Tamir et al., 2012): 1/200; mouse anti-α-tubulin (12G10, DSHB; (Thazhath et al., 2002)): 1/250; rat anti-Koi (Kracklauer et al., 2007): 1/100; mouse anti-ATP5A (abcam, ab14748); chicken anti-GFP (Abcam, 1:1000); mouse anti-mitochondria (abcam, ab92824 1:1000). The following dyes were added along with secondary antibodies: phalloidin, conjugated with Alexa-549, Alexa-488 or Alexa-649 (Thermo Scientific): 1/100

and DAPI (Thermo Scientific): 1/1000. Samples were mounted in Vectashield (Vector Laboratories) or Prolong Diamond Antifade Mountant (Thermo Fisher, # P36961) prior to imaging with a confocal microscope (Leica SP8 or Zeiss 880).

Electron Microscopy—Third instar larvae were dissected in HL3 (Stewart et al., 1994), containing 0.5mM Ca^{2+}. Subsequently, tissues were fixed (4% paraformaldehyde, 2% glutaraldehyde, 0.1 M sodium cacodylate (pH 7.2) and 0.5mM Ca^{2+}) overnight at 4°C, post-fixed in 1% OsO_4 for 2×1min, dehydrated in ethanol and propylene oxide, and embedded in Embed-812 resin (Electron Microscopy Sciences). Sections (~50 nm) were stained in 4% uranyl acetate and 2.5% lead nitrate, and TEM images were captured using a transmission electron microscope (model 1010, JEOL). Per genotype, images were obtained from three animals.

Protein purification—pGEX-4T1_ari-1 and parkin (WT/RBR/OCD/OPEN/$OPEN^A$/$OPEN^B$) and pET28a_KoiU2 constructs were transformed into BL21-DE3 cells (NEB). Various Ari-1 constructs were expressed in LB, supplemented with 0.05mM IPTG and 0.2mM ZnCl2, for 22 hours in 18°C shaking. Cells were lysed with Bugbuster (Novagen). Proteins were purified following established protocols (Wenzel et al., 2011) with column packed with Gluthathione Sepharose 4B (Biorad, GE Healthcare). KoiU2 was expressed in LB supplemented with 0.05mM IPTG for 22 hours in 18°C. Proteins were purified using Ni2+-NTA column (Qiagen, Biorad) and eluted with 500mM imidazole. Proteins were subsequently dialyzed against 50mM Tris pH8.0, 200mM NaCl to remove imidazole.

***In vitro* ubiquitination—**A 50 μL reaction mixture for KoiU2 ubiquitination contained 1μM human E1 recombinant protein (Enzo), 5μM UbcH7 (Boston Biochem), 2μM GST-tagged E3 ubiquitin ligase, 5μM T7-KoiU2, 5mM Mg-ATP (Enzo) 2.5μM biotinylated ubiquitin (Enzo) and 1mM DTT in 1× ubiquitination buffer (Enzo). Reactions were assembled at 4°C and initiated at 37°C. Ubiquitination reactions were stopped after one hour by adding 1× Laemlli buffer, after which the samples were boiled for 5 minutes before being loaded onto the SDS-PAGE gel for analysis.

QUANTIFICATION AND STATISTICAL ANALYSIS

Electron Microscopy—For each genotype, images were obtained from 3 animals and at least 10 images were analyzed per genotype. Images were processed with ImageJ and Adobe Photoshop. Aspect Ratio, circularity and area of indicated structures were analyzed using Fiji (ImageJ).

Immunohistochemistry—Measurement of nuclear Koi levels was performed on 3D images. An image containing a z-stack through the entire nucleus was opened in Imaris. Next, a “spot”, a 3D feature of Imaris that overlays a ball-shaped object the size of the nucleus in that image, was created. The average intensity of Koi within this shape was measured. Subsequently, a second “spot” with the same dimensions as the first one was placed on a part of the image that does not contain the nucleus in order to measure the background intensity of the antibody. The intensity of this second spot was subtracted from Koi’s average intensity of the first spot.

This way, measurements were made for every image and every genotype. Based on these measurements, we calculated the average nuclear Koi intensity that is present in control animals. Finally, we normalized every measurement to the average control Koi Intensity to reach the numbers shown in graph 3B.

Co-immunoprecipitation and western Blot analysis—Experiments were repeated at least three times. ImageJ's Gel Analysis method or ImageStudioLite were used to quantify band intensities. The average intensity was quantified and represented ± SD in bar graphs.

Statistics and Error bars—For *Drosophila in vivo* studies, sample sizes are stated in the figure legends. For percentage of nuclear clustering analyses, 'n' stated in graphs are number of A3M6 muscles analyzed. For other experiments, 'n' indicates distinct samples (animals or cells). Due to the high cost associated with electron microscopic analyses, a smaller sample size was analyzed, but a large number of nuclei were quantified for each sample.

Error bars in each graph represent either mean ± SD or mean ± SEM, as stated in the figure legends.

Statistical analysis: Statistics were quantified using GraphPad PRISM 7, using either unpaired t-tests or One-Way ANOVA with Tukey post-tests as stated in figure legends. Statistical significance is shown in figure legends.

KEY RESOURCES TABLE

Please refer to Key Resources Table for specific materials used.

REAGENT or RESOURCE	SOURCE	IDENTIFIER
Antibodies		
chicken polyclonal anti-GFP	Abcam	CAT#ab13970; RRID: AB_300798
mouse monoclonal anti-LamC	Developmental Studies Hybridoma Bank (DSHB)	CAT#LC28.26; RRID: AB_528339
rabbit polyclonal anti-GFP	Life technologies	CAT#A11122; RRID: AB_221569
guinea pig polyclonal anti-Msp-300	Elhanany-Tamir et al., 2012	AB_2570007
rat polyclonal anti-Koi	Kracklauer et al., 2007	AB_2632403
mouse monoclonal anti-actin	Milipore	CAT#C4; RRID: AB_2223041
mouse monoclonal anti-V5	Thermo Scientific	CAT#R960-25; RRID: AB_2556564
mouse monoclonal anti-HA	Covance	CAT#16B12; RRID: AB_10064220
mouse monoclonal anti-Flag	Sigma	CAT#F1804; RRID: AB_262044
mouse monoclonal anti-ATP5A	Thermo Scientific	CAT#15H4C4; RRID: AB_2533548
mouse polyclonal anti-LaminA/C	Cell signaling	CAT#4777; RRID: AB_10545756
rabbit polyclonal anti-T7	Novus Biologicals	CAT#NB600-372; RRID: AB_10002902
goat GST antibody	GE Healthcare	CAT#27-4577-01; RRID: AB_771432
Phalloidin 488nm	Thermo Scientific	CAT#A12379; RRID: AB_2315147

REAGENT or RESOURCE	SOURCE	IDENTIFIER
TOPRO3	Thermo Scientific	CAT#T3605
DAPI	Thermo Scientific	CAT#D1306; RRID: AB_2629482
Biological Samples		
Control human aortic tissue 1	This study (donor)	
Control human aortic tissue 2	This study (donor)	
R171X human aortic tissue	This study (patient)	
E15Q human aortic tissue	This study (patient)	
Chemicals, Peptides, and Recombinant Proteins		
Prolong Diamond Antifade Mountant	Thermo Fisher	CAT#P36961
Vectashield	Vector Labs	CAT#H-1000
Pierce™ Protease Inhibitor Tablets, EDTA-free	Thermo Scientific	CAT#88266
Schneider's Drosophila medium	Thermo Scientific	CAT#21720
Fetal Bovine Serum, Heat-inactivated	Sigma-Aldrich	CAT#F4135
Penicilin Streptomycin	Thermo Scientific	CAT#15070063
Cell lysis buffer	Cell signaling	CAT#9803
Smooth muscle growth medium-2	Lonza	CAT#CC-3182
Fetal Bovine Serum (for vSMC study)	Atlanta Biologicals	CAT#S11195
TGF-β1	R&D systems	CAT#P01137
Cacodylic Acid, Trihydrate Sodium 100g	EMS	CAT#12300
EM-grade glutaraldehyde, 25% Aq solution	EMS	CAT#16221
Osmium tetroxide 4% Aq solution	EMS	CAT#19191
Paraformaldehyde 16% Aq Solution	EMS	CAT#15711
Propylene Oxide	EMS	CAT#20411
Koptec 200 Proof 100% ethanol Anhydrous	VWR	CAT#89125-186
Embed-812	EMS	CAT#14901
NMA	EMS	CAT#19001
DDSA	EMS	CAT#13711
DMP-30	EMS	CAT#13600
Uranyl Acetate	EMS	CAT#RT22400
Lead Nitrate	EMS	CAT#RT17900-25
Cycloheximide	Sigma-Aldrich	CAT#C4859
MG-132	Sigma-Aldrich	CAT#M7449
Ubiquitin activating enzyme E1 (human)	Enzo	CAT#BML-UW9410-0050
UbcH7/UBE2L3	BostonBiochem	CAT#E2-640
10x Ubiquitinylation Buffer	Enzo	CAT#BML-KW9885-0005
Mg2+/ATP Activating Solution	Enzo	CAT#BML-EW9805-0100
1,4-Dithiothreitol	Sigma-Aldrich	CAT#10197777001
Ari-1-GST	this study	
ARIH1 RBR-GST	this study	

REAGENT or RESOURCE	SOURCE	IDENTIFIER
Ari-1 DEAD-GST	this study	
Ari-1 OPEN-GST	this study	
Ari-1 OPEN^{A}-GST	this study	
Ari-1 OPEN^{B}-GST	this study	
Parkin-RBR-GST	this study	
Critical Commercial Assays		
Effectene Transfection Reagent	Qiagen	CAT#301425
High-Capacity cDNA Reverse Transcription Kit	Applied Biosystems, Thermo Scientific	CAT #4368814
iTaq™ Universal SYBR® Green Supermix	Bio Rad	CAT #1725121
ATP/ADP ratio	Abcam	CAT #ab65313
Chromotek-GFP-Trap Agarose Beads	Allele biotechnology	CAT #ACT-CM-GFA0050
Anti-V5 Agarose Affinity Gel	Sigma-Aldrich	CAT #A7345; RRID: AB_10062721
Anti-FLAG® M2 Affinity Gel	Sigma-Aldrich	CAT #A2220; RRID: AB_10063035
EZview™ Red Anti-HA Affinity Gel	Sigma-Aldrich	CAT #E6779; RRID: AB_10109562
T7 tag antibody agarose	EMD Millipore	CAT #69026-3; RRID: AB_10947861
QuikChange Lightning Site-Directed Mutagenesis Kit	Agilent technologies	CAT#210518
Lipofectamine 3000	Thermo Scientific	CAT# L3000001
HRP-Streptavidin	Jackson Immunoresearch	CAT #016-030-084; RRID: AB_2337238
Experimental Models: Cell Lines		
D. melanogaster: Cell line S2: S2-DRSC	laboratory of Norbert Perrimon	FlyBase: FBtc0000181
Immortalized human primary vSMC	Guo et al., 2016	#11023
HEK293T (viral packaging)	Dharmacon	CAT#HCL4517
Experimental Models: Organisms/Strains		
D. melanogaster: Duplication covering *ari-1: Df(1)osUE69/C(1)DX, y1 f1/Dp(1;Y)W39, y+*	Bloomington Drosophila Stock Center	BDSC_1538
D. melanogaster: Duplication covering *ari-1: w1118; Dp(1;3)DC342, PBac{DC342}VK00033*	Bloomington Drosophila Stock Center	BDSC_30756
y w ; P[(w+) UAS-ari-1+	(Gradilla et al., 2011)	
y w ; P[(w+)UAS-ARIH1] / CyO	Gift from Alberto Ferrus	
P{Gal4-da.G32}UH1	Bloomington Drosophila Stock Center	BDSC_55850
P{GAL4-Mef2.R}3	Bloomington Drosophila Stock Center	BDSC_27390
Df(1)BSC352, w1118/FM7h/Dp(2;Y)G	Bloomington Drosophila Stock Center	BDSC_24376
w1118; Df(2R)Exel6050, P{XP-U}Exel6050/CyO	Bloomington Drosophila Stock Center	BDSC_7532
w1118; Df(2R)BSC347/CyO	Bloomington Drosophila Stock Center	BDSC_24371
w; P{GawB}Ubc10^{NP2336} / CyO*	Kyoto Stock Center	

REAGENT or RESOURCE	SOURCE	IDENTIFIER
w^{1118}; P{w[+mGT]=GT1}$Ubc10^{BG00902}$/CyO	Bloomington Drosophila Stock Center	BDSC_12444
cl(1) P{neoFRT}19A/ Dp(1;Y)y+ v+ ey-FLP*	(Newsome et al., 2000)	
koi84	(Kracklauer et al., 2007)	
w; park$\hat{}$"^{21}/TM3, P{GAL4-Kr.C}DC2, P{UAS-GFP.S65T}DC10, Sb1*	Bloomington Drosophila Stock Center	BDSC_51652
$park^{13}$ / TM6B	(Greene et al., 2003)	
PBac{WH}parkf01950	Exelixis at Harvard Medical School. (Thibault et al, 2004)	FlyBase_FBst1017381
y1 w, P{neoFRT}19A iso*	(Yamamoto et al., 2014)	
y^1 w* ari-1^A P{neoFRT}19A/FM7c, P{GAL4-Kr.C}DC1, P{UAS-GFP.S65T}DC5, sn^+	(Haelterman et al., 2014a)	
y^1 w* ari-1^B P{neoFRT}19A/FM7c, P{GAL4-Kr.C}DC1, P{UAS-GFP.S65T}DC5, sn^+	(Haelterman et al., 2014a)	
y^1 w* ari-1^D P{neoFRT}19A/FM7c, P{GAL4-Kr.C}DC1, P{UAS-GFP.S65T}DC5, sn^+	(Haelterman et al., 2014a)	
y w* ari-$1^{CRI\{MIC\}}$ /FM7c, P{GAL4-Kr.C}DC1, P{UAS-GFP.S65T}DC5, sn+*	This study	
y w* ari-$1^{CRI\{GFSTF\}}$*	This study	
y w* ari-$1^{CRI\{T2A-GAL4\}}$* /FM7c	This study	
y w ; P[(w+)UASattB-$ARIH1^{R171*}$] VK37 / CyO	This study	
y w ; P[(w+)UASattB-$ARIH1^{E44G}$] VK37 / CyO	This study	
y w ; P[(w+)UASattB-ari-2-V5] VK37 / CyO	This study	
y^2 cho^2 v^1; attP40{nos-Cas9}/CyO	NIG-FLY	CAT#CAS0001
Oligonucleotides (Refer to supplementary table)		
Recombinant DNA		
plasmid: pMK33-stim-C-FLAG-HA	(Guruharsha et al., 2011)	
plasmid: pMK33-koi-C-FLAG-HA	(Guruharsha et al., 2011)	
plasmid: pMK33-klar-C-FLAG-HA	(Guruharsha et al., 2011)	
plasmid: pMK33-Msp300-C-FLAG-HA	(Guruharsha et al., 2011)	
plasmid: pUAS_ensconsin-HA	(Metzger et al., 2012)	
plasmid: pFLC-I _ari-1	Berkeley Drosophila Genome Project	BDGP: RE69116
Plasmid: pOT2-park	Berkeley Drosophila Genome Project	BDGP: SD01679
plasmid: pFLC-I _ubc10	Berkeley Drosophila Genome Project	BDGP: RE47264
plasmid: pFLC-I _koiNterm	Berkeley Drosophila Genome Project	BDGP: RE12054
plasmid: pCR2.1_koiCterm	Berkeley Drosophila Genome Project	BDGP: RT06825
plasmid: pCMV-SPORT6_ARIH1	Harvard PlasmID Database	REF#: HsCD00338442
plasmid: pCFD3:U6:3-gRNA	Addgene, (Port et al., 2014)	CAT#49410

REAGENT or RESOURCE	SOURCE	IDENTIFIER
plasmid: pLKO.1-EGFP	modified in Guo et al., 2016	
plasmid: pUASTattb_ari-1*N-V5	This study	
plasmid: pUASTattb_ari-1-N-HA	This study	
plasmid: pUASTattb_ari-2-N-Flag	This study	
plasmid: pUASTattb_ari-2-N-V5	This study	
plasmid: pUASTattb_park-N-Flag	This study	
plasmid: pUASTattb_park-N-HA	This study	
plasmid: pUASTattb_KoiNterm-N-GFP	This study	
plasmid: pUASTattb_UbcD10-C-GFP	This study	
plasmid: pUASTattb_ARIH1*	This study	
plasmid: pGEX4T1-ari-1*	This study	
plasmid: pGEX4T1-ari-1 RBR	Addgene; Wenzel et al., 2011	CAT#31254
plasmid: pGEX4T2-parkin RBR	Addgene; Wenzel et al., 2012	CAT#31255
plasmid: pET28a-KoiU2	This study	
plasmid: pUASTattb_UbcD10-C-GFP	This study	
plasmid: pUASTattb_ARIH1*	This study	
Other		
ARIH1 gipz lentiviral shRNA (03)	GE Dharmacon	cloneID: V3LHS_334303
ARIH1 gipz lentiviral shRNA (05)	GE Dharmacon	cloneID: V2LHS_199505
ARIH1 gipz lentiviral shRNA (15)	GE Dharmacon	cloneID: V2LHS_199015
GFP dsRNA	this study	
ari-1-1 dsRNA	this study	
ari-1-2 dsRNA	this study	

Supplementary Material

Refer to Web version on PubMed Central for supplementary material.

Acknowledgments

We want to thank the families participating in this research. We thank the BDSC (NIH P40OD018537), DGRC, BDGP, and the Developmental Studies Hybridoma Bank for flies, molecular biology reagents and antibodies. We are grateful to Alberto Ferrus, Sheng Zhang, Janice Fischer, Spyros Artavanis-Tsakonas, Mary Baylies, Talila Volk and Gabriel Vasquez-Velez for sharing fly stocks, molecular biology reagents and antibodies. We thank Katherine Reiter and Rachel Klevit for valuable advice on Ari-1/RBR purification. We thank Herman Dierick, Berrak Ugur, Juan Botas, Michael Galko, Hamed Jafar-Nejad, Kartik Venkatachalam, Meng Wang and Nikolaos Giagtzoglou for helpful discussions and comments. We thank Wen-Wen Lin for generating the *ari-1*^{T2A} line. We thank Honglin Pan and Yuchun He for injections to create transgenic flies. H.J.B. is an investigator of the Howard Hughes Medical Institute. This work was supported in part by NIH grants R24OD022005, and R01GM067858 to H.J.B; by the National Heart, Lung and Blood Institute (RO1 HL109942 and P01HL110869), the John Ritter Foundation, and the Henrietta B. and Frederick H. Bugher Foundation to D.M.M. Sequencing was provided by the University of Washington Center for Mendelian Genomics (UW-CMG) and was funded by the National Human Genome Research Institute and the National Heart, Lung and Blood Institute grant UM1HG006493 to Drs. Debbie Nickerson, Michael Bamshad, and Suzanne Leal.

References

Aguilera M, Oliveros M, Martinez-Padron M, Barbas JA, Ferrus A. Ariadne-1: a vital Drosophila gene is required in development and defines a new conserved family of ring-finger proteins. Genetics. 2000; 155(3):1231–44. [PubMed: 10880484]

Alam SG, Zhang Q, Prasad N, Li Y, Chamala S, Kuchibhotla R, Kc B, Aggarwal V, Shrestha S, Jones AL, et al. The mammalian LINC complex regulates genome transcriptional responses to substrate rigidity. Sci Rep. 2016; 6:38063. [PubMed: 27905489]

Arsenovic PT, Ramachandran I, Bathula K, Zhu R, Narang JD, Noll NA, Lemmon CA, Gundersen GG, Conway DE. Nesprin-2G, a Component of the Nuclear LINC Complex, Is Subject to Myosin-Dependent Tension. Biophys J. 2016; 110(1):34–43. [PubMed: 26745407]

Bischof J, Bjorklund M, Furger E, Schertel C, Taipale J, Basler K. A versatile platform for creating a comprehensive UAS-ORFeome library in Drosophila. Development. 2013; 140(11):2434–42. [PubMed: 23637332]

Bone CR, Starr DA. Nuclear migration events throughout development. J Cell Sci. 2016; 129(10): 1951–61. [PubMed: 27182060]

Bonne G, Di Barletta MR, Varnous S, Becane HM, Hammouda EH, Merlini L, Muntoni F, Greenberg CR, Gary F, Urtizberea JA, et al. Mutations in the gene encoding lamin A/C cause autosomal dominant Emery-Dreifuss muscular dystrophy. Nat Genet. 1999; 21(3):285–8. [PubMed: 10080180]

Brand AH, Perrimon N. Targeted gene expression as a means of altering cell fates and generating dominant phenotypes. Development. 1993; 118(2):401–15. [PubMed: 8223268]

Buszczak M, Paterno S, Lighthouse D, Bachman J, Planck J, Owen S, Skora AD, Nystul TG, Ohlstein B, Allen A, et al. The carnegie protein trap library: a versatile tool for Drosophila developmental studies. Genetics. 2007; 175(3):1505–31. [PubMed: 17194782]

Chang W, Worman HJ, Gundersen GG. Accessorizing and anchoring the LINC complex for multifunctionality. J Cell Biol. 2015; 208(1):11–22. [PubMed: 25559183]

Chen CY, Chi YH, Mutalif RA, Starost MF, Myers TG, Anderson SA, Stewart CL, Jeang KT. Accumulation of the inner nuclear envelope protein Sun1 is pathogenic in progeric and dystrophic laminopathies. Cell. 2012; 149(3):565–77. [PubMed: 22541428]

Chintapalli VR, Wang J, Dow JA. Using FlyAtlas to identify better Drosophila melanogaster models of human disease. Nat Genet. 2007; 39(6):715–20. [PubMed: 17534367]

Coyaud E, Mis M, Laurent EM, Dunham WH, Couzens AL, Robitaille M, Gingras AC, Angers S, Raught B. BioID-based Identification of Skp Cullin F-box (SCF)β-TrCP1/2 E3 Ligase Substrates. Mol Cell Proteomics. 2015; 14(7):1781–95. [PubMed: 25900982]

Deshaies RJ, Joazeiro CA. RING domain E3 ubiquitin ligases. Annu Rev Biochem. 2009; 78:399–434. [PubMed: 19489725]

Diao F, Ironfield H, Luan H, Diao F, Shropshire WC, Ewer J, Marr E, Potter CJ, Landgraf M, White BH. Plug-and-play genetic access to drosophila cell types using exchangeable exon cassettes. Cell Rep. 2015; 10(8):1410–21. [PubMed: 25732830]

Duda DM, Olszewski JL, Schuermann JP, Kurinov I, Miller DJ, Nourse A, Alpi AF, Schulman BA. Structure of HHARI, a RING-IBR-RING ubiquitin ligase: autoinhibition of an Ariadne-family E3 and insights into ligation mechanism. Structure. 2013; 21(6):1030–41. [PubMed: 23707686]

Eisenhaber B, Chumak N, Eisenhaber F, Hauser MT. The ring between ring fingers (RBR) protein family. Genome Biol. 2007; 8(3):209. [PubMed: 17367545]

Elhanany-Tamir H, Yu YV, Shnayder M, Jain A, Welte M, Volk T. Organelle positioning in muscles requires cooperation between two KASH proteins and microtubules. J Cell Biol. 2012; 198(5): 833–46. [PubMed: 22927463]

Foe VE, Alberts BM. Studies of nuclear and cytoplasmic behaviour during the five mitotic cycles that precede gastrulation in Drosophila embryogenesis. J Cell Sci. 1983; 61:31–70. [PubMed: 6411748]

Folker ES, Baylies MK. Nuclear positioning in muscle development and disease. Front Physiol. 2013; 4:363. [PubMed: 24376424]

Geisler S, Holmstrom KM, Skujat D, Fiesel FC, Rothfuss OC, Kahle PJ, Springer W. PINK1/Parkin-mediated mitophagy is dependent on VDAC1 and p62/SQSTM1. Nat Cell Biol. 2010; 12(2):119–31. [PubMed: 20098416]

Gnerer JP, Venken KJ, Dierick HA. Gene-specific cell labeling using MiMIC transposons. Nucleic Acids Res. 2015; 43(8):e56. [PubMed: 25712101]

Goldberg MS, Fleming SM, Palacino JJ, Cepeda C, Lam HA, Bhatnagar A, Meloni EG, Wu N, Ackerson LC, Klapstein GJ, et al. Parkin-deficient mice exhibit nigrostriatal deficits but not loss of dopaminergic neurons. J Biol Chem. 2003; 278(44):43628–35. [PubMed: 12930822]

Gradilla AC, Mansilla A, Ferrus A. Isoform-specific regulation of a steroid hormone nuclear receptor by an E3 ubiquitin ligase in Drosophila melanogaster. Genetics. 2011; 189(3):871–83. [PubMed: 21900267]

Greene JC, Whitworth AJ, Kuo I, Andrews LA, Feany MB, Pallanck LJ. Mitochondrial pathology and apoptotic muscle degeneration in Drosophila parkin mutants. Proc Natl Acad Sci U S A. 2003; 100(7):4078–83. [PubMed: 12642658]

Gros-Louis F, Dupre N, Dion P, Fox MA, Laurent S, Verreault S, Sanes JR, Bouchard JP, Rouleau GA. Mutations in SYNE1 lead to a newly discovered form of autosomal recessive cerebellar ataxia. Nat Genet. 2007; 39(1):80–5. [PubMed: 17159980]

Guilluy C, Burridge K. Nuclear mechanotransduction: forcing the nucleus to respond. Nucleus. 2015; 6(1):19–22. [PubMed: 25738642]

Guo DC, Duan XY, Regalado ES, Mellor-Crummey L, Kwartler CS, Kim D, Lieberman K, de Vries BB, Pfundt R, Schinzel A, et al. Loss-of-Function Mutations in YY1AP1 Lead to Grange Syndrome and a Fibromuscular Dysplasia-Like Vascular Disease. Am J Hum Genet. 2017; 100(1): 21–30. [PubMed: 27939641]

Guo DC, Pannu H, Tran-Fadulu V, Papke CL, Yu RK, Avidan N, Bourgeois S, Estrera AL, Safi HJ, Sparks E, et al. Mutations in smooth muscle alpha-actin (ACTA2) lead to thoracic aortic aneurysms and dissections. Nat Genet. 2007; 39(12):1488–93. [PubMed: 17994018]

Guo DC, Regalado E, Casteel DE, Santos-Cortez RL, Gong L, Kim JJ, Dyack S, Horne SG, Chang G, Jondeau G, et al. Recurrent gain-of-function mutation in PRKG1 causes thoracic aortic aneurysms and acute aortic dissections. Am J Hum Genet. 2013; 93(2):398–404. [PubMed: 23910461]

Guruharsha KG, Rual JF, Zhai B, Mintseris J, Vaidya P, Vaidya N, Beekman C, Wong C, Rhee DY, Cenaj O, et al. A protein complex network of Drosophila melanogaster. Cell. 2011; 147(3):690–703. [PubMed: 22036573]

Haelterman NA, Jiang L, Li Y, Bayat V, Sandoval H, Ugur B, Tan KL, Zhang K, Bei D, Xiong B, et al. Large-scale identification of chemically induced mutations in Drosophila melanogaster. Genome Res. 2014a; 24(10):1707–18. [PubMed: 25258387]

Haelterman NA, Yoon WH, Sandoval H, Jaiswal M, Shulman JM, Bellen HJ. A mitocentric view of Parkinson's disease. Annu Rev Neurosci. 2014b; 37:137–59. [PubMed: 24821430]

Horn HF, Brownstein Z, Lenz DR, Shivatzki S, Dror AA, Dagan-Rosenfeld O, Friedman LM, Roux KJ, Kozlov S, Jeang KT, et al. The LINC complex is essential for hearing. J Clin Invest. 2013; 123(2):740–50. [PubMed: 23348741]

Khau Van Kien P, Mathieu F, Zhu L, Lalande A, Betard C, Lathrop M, Brunotte F, Wolf JE, Jeunemaitre X. Mapping of familial thoracic aortic aneurysm/dissection with patent ductus arteriosus to 16p122-p1313. Circulation. 2005; 112(2):200–6. [PubMed: 15998682]

Kim DH, Cho S, Wirtz D. Tight coupling between nucleus and cell migration through the perinuclear actin cap. J Cell Sci. 2014; 127(Pt 11):2528–41. [PubMed: 24639463]

Kim DI, Birendra KC, Roux KJ. Making the LINC: SUN and KASH protein interactions. Biol Chem. 2015; 396(4):295–310. [PubMed: 25720065]

Koizumi H, Higginbotham H, Poon T, Tanaka T, Brinkman BC, Gleeson JG. Doublecortin maintains bipolar shape and nuclear translocation during migration in the adult forebrain. Nat Neurosci. 2006; 9(6):779–86. [PubMed: 16699506]

Kracklauer MP, Banks SM, Xie X, Wu Y, Fischer JA. Drosophila klaroid encodes a SUN domain protein required for Klarsicht localization to the nuclear envelope and nuclear migration in the eye. Fly (Austin). 2007; 1(2):75–85. [PubMed: 18820457]

Kracklauer MP, Wiora HM, Deery WJ, Chen X, Bolival B Jr, Romanowicz D, Simonette RA, Fuller MT, Fischer JA, Beckingham KM. The Drosophila SUN protein Spag4 cooperates with the coiled-coil protein Yuri Gagarin to maintain association of the basal body and spermatid nucleus. J Cell Sci. 2010; 123(Pt 16):2763–72. [PubMed: 20647369]

Lek M, Karczewski KJ, Minikel EV, Samocha KE, Banks E, Fennell T, O'Donnell-Luria AH, Ware JS, Hill AJ, Cummings BB, et al. Analysis of protein-coding genetic variation in 60,706 humans. Nature. 2016; 536(7616):285–91. [PubMed: 27535533]

Lucking CB, Durr A, Bonifati V, Vaughan J, De Michele G, Gasser T, Harhangi BS, Meco G, Denefle P, Wood NW, et al. Association between early-onset Parkinson's disease and mutations in the parkin gene. N Engl J Med. 2000; 342(21):1560–7. [PubMed: 10824074]

Meinke P, Mattioli E, Haque F, Antoku S, Columbaro M, Straatman KR, Worman HJ, Gundersen GG, Lattanzi G, Wehnert M, et al. Muscular dystrophy-associated SUN1 and SUN2 variants disrupt nuclear-cytoskeletal connections and myonuclear organization. PLoS Genet. 2014; 10(9):e1004605. [PubMed: 25210889]

Metzger T, Gache V, Xu M, Cadot B, Folker ES, Richardson BE, Gomes ER, Baylies MK. MAP and kinesin-dependent nuclear positioning is required for skeletal muscle function. Nature. 2012; 484(7392):120–4. [PubMed: 22425998]

Milewicz DM, Trybus KM, Guo D, Sweeney HL, Regalado E, Kamm K, Stull JT. Altered Smooth Muscle Cell Force Generation as a Driver of Thoracic Aortic Aneurysms and Dissections. Arterioscler Thromb Vasc Biol. 2016

Nagarkar-Jaiswal S, DeLuca SZ, Lee PT, Lin WW, Pan H, Zuo Z, Lv J, Spradling AC, Bellen HJ. A genetic toolkit for tagging intronic MiMIC containing genes. Elife. 2015a; 4

Nagarkar-Jaiswal S, Lee PT, Campbell ME, Chen K, Anguiano-Zarate S, Gutierrez MC, Busby T, Lin WW, He Y, Schulze KL, et al. A library of MiMICs allows tagging of genes and reversible, spatial and temporal knockdown of proteins in Drosophila. Elife. 2015b; 4

Narendra D, Tanaka A, Suen DF, Youle RJ. Parkin is recruited selectively to impaired mitochondria and promotes their autophagy. J Cell Biol. 2008; 183(5):795–803. [PubMed: 19029340]

Navarro AP, Collins MA, Folker ES. The nucleus is a conserved mechanosensation and mechanoresponse organelle. Cytoskeleton (Hoboken). 2016; 73(2):59–67. [PubMed: 26849407]

Neelam S, Chancellor TJ, Li Y, Nickerson JA, Roux KJ, Dickinson RB, Lele TP. Direct force probe reveals the mechanics of nuclear homeostasis in the mammalian cell. Proc Natl Acad Sci U S A. 2015; 112(18):5720–5. [PubMed: 25901323]

Newsome TP, Asling B, Dickson BJ. Analysis of Drosophila photoreceptor axon guidance in eye-specific mosaics. Development. 2000; 127(4):851–60. [PubMed: 10648243]

Palacino JJ, Sagi D, Goldberg MS, Krauss S, Motz C, Wacker M, Klose J, Shen J. Mitochondrial dysfunction and oxidative damage in parkin-deficient mice. J Biol Chem. 2004; 279(18):18614–22. [PubMed: 14985362]

Parelkar SS, Cadena JG, Kim C, Wang Z, Sugal R, Bentley B, Moral L, Ardley HC, Schwartz LM. The parkin-like human homolog of Drosophila ariadne-1 (HHARI) can induce aggresome formation in mammalian cells and is immunologically detectable in Lewy bodies. J Mol Neurosci. 2012; 46(1): 109–21. [PubMed: 21590270]

Pesah Y, Pham T, Burgess H, Middlebrooks B, Verstreken P, Zhou Y, Harding M, Bellen H, Mardon G. Drosophila parkin mutants have decreased mass and cell size and increased sensitivity to oxygen radical stress. Development. 2004; 131(9):2183–94. [PubMed: 15073152]

Port F, Chen HM, Lee T, Bullock SL. Optimized CRISPR/Cas tools for efficient germline and somatic genome engineering in Drosophila. Proc Natl Acad Sci U S A. 2014; 111(29):E2967–76. [PubMed: 25002478]

Radivojac P, Vacic V, Haynes C, Cocklin RR, Mohan A, Heyen JW, Goebl MG, Iakoucheva LM. Identification, analysis, and prediction of protein ubiquitination sites. Proteins. 2010; 78(2):365–80. [PubMed: 19722269]

Riemer D, Stuurman N, Berrios M, Hunter C, Fisher PA, Weber K. Expression of Drosophila lamin C is developmentally regulated: analogies with vertebrate A-type lamins. J Cell Sci. 1995; 108(Pt 10):3189–98. [PubMed: 7593280]

Scott DC, Rhee DY, Duda DM, Kelsall IR, Olszewski JL, Paulo JA, de Jong A, Ovaa H, Alpi AF, Harper JW, et al. Two Distinct Types of E3 Ligases Work in Unison to Regulate Substrate Ubiquitylation. Cell. 2016; 166(5):1198–1214 e24. [PubMed: 27565346]

Sijacic P, Wang W, Liu Z. Recessive antimorphic alleles overcome functionally redundant loci to reveal TSO1 function in Arabidopsis flowers and meristems. PLoS Genet. 2011; 7(11):e1002352. [PubMed: 22072982]

Simon DN, Wilson KL. Partners and post-translational modifications of nuclear lamins. Chromosoma. 2013; 122(1–2):13–31. [PubMed: 23475188]

Sobreira N, Schiettecatte F, Valle D, Hamosh A. GeneMatcher: a matching tool for connecting investigators with an interest in the same gene. Hum Mutat. 2015; 36(10):928–30. [PubMed: 26220891]

Spear PC, Erickson CA. Interkinetic nuclear migration: a mysterious process in search of a function. Dev Growth Differ. 2012; 54(3):306–16. [PubMed: 22524603]

Stephenson, S., Taylor, J., Lockhart, PJ. Parkinson's Disease and Parkin: Insights from Park2 Knockout Mice. In: Dushanova, J., editor. Mechanisms in Parkinson's Disease - Models and Treatments". 2012.

Stewart BA, Atwood HL, Renger JJ, Wang J, Wu CF. Improved stability of Drosophila larval neuromuscular preparations in haemolymph-like physiological solutions. J Comp Physiol A. 1994; 175(2):179–91. [PubMed: 8071894]

Thazhath R, Liu C, Gaertig J. Polyglycylation domain of beta-tubulin maintains axonemal architecture and affects cytokinesis in Tetrahymena. Nat Cell Biol. 2002; 4(3):256–9. [PubMed: 11862218]

Thibault ST, Singer MA, Miyazaki WY, Milash B, Dompe NA, Singh CM, Buchholz R, Demsky M, Fawcett R, Francis-Lang HL, et al. A complementary transposon tool kit for Drosophila melanogaster using P and piggyBac. Nat Genet. 2004; 36(3):283–7. [PubMed: 14981521]

Venken KJ, He Y, Hoskins RA, Bellen HJ. P[acman]: a BAC transgenic platform for targeted insertion of large DNA fragments in D. melanogaster. Science. 2006; 314(5806):1747–51. [PubMed: 17138868]

Venken KJ, Popodi E, Holtzman SL, Schulze KL, Park S, Carlson JW, Hoskins RA, Bellen HJ, Kaufman TC. A molecularly defined duplication set for the X chromosome of Drosophila melanogaster. Genetics. 2010; 186(4):1111–25. [PubMed: 20876565]

Venken KJ, Schulze KL, Haelterman NA, Pan H, He Y, Evans-Holm M, Carlson JW, Levis RW, Spradling AC, Hoskins RA, et al. MiMIC: a highly versatile transposon insertion resource for engineering Drosophila melanogaster genes. Nat Methods. 2011; 8(9):737–43. [PubMed: 21985007]

Volk T, Wang S. Protection of muscle nuclei. Oncotarget. 2015; 6(27):23046–7. [PubMed: 26309083]

Von Coelln R, Thomas B, Savitt JM, Lim KL, Sasaki M, Hess EJ, Dawson VL, Dawson TM. Loss of locus coeruleus neurons and reduced startle in parkin null mice. Proc Natl Acad Sci U S A. 2004; 101(29):10744–9. [PubMed: 15249681]

Vos M, Esposito G, Edirisinghe JN, Vilain S, Haddad DM, Slabbaert JR, Van Meensel S, Schaap O, De Strooper B, Meganathan R, et al. Vitamin K2 is a mitochondrial electron carrier that rescues pink1 deficiency. Science. 2012; 336(6086):1306–10. [PubMed: 22582012]

Wang J, R A-O, Hu Y, Kim SY, Wan YW, Wangler MF, Yamamoto S, Chao HT, Comjean A, Mohr SE, et al. MARRVEL: Integration of Human and Model Organism Genetic Resources to Facilitate Functional Annotation of the Human Genome. Am J Hum Genet. 2017

Wang L, Guo DC, Cao J, Gong L, Kamm KE, Regalado E, Li L, Shete S, He WQ, Zhu MS, Offermanns S, et al. Mutations in myosin light chain kinase cause familial aortic dissections. Am J Hum Genet. 2010; 87(5):701–7. [PubMed: 21055718]

Wenzel DM, Lissounov A, Brzovic PS, Klevit RE. UBCH7 reactivity profile reveals parkin and HHARI to be RING/HECT hybrids. Nature. 2011; 474(7349):105–8. [PubMed: 21532592]

Yamamoto S, Jaiswal M, Charng WL, Gambin T, Karaca E, Mirzaa G, Wiszniewski W, Sandoval H, Haelterman NA, Xiong B, et al. A drosophila genetic resource of mutants to study mechanisms underlying human genetic diseases. Cell. 2014; 159(1):200–14. [PubMed: 25259927]

Yu C, Wan KH, Hammonds AS, Stapleton M, Carlson JW, Celniker SE. Development of expression-ready constructs for generation of proteomic libraries. Methods Mol Biol. 2011; 723:257–72. [PubMed: 21370071]

Zesiewicz TA, Strom JA, Borenstein AR, Hauser RA, Cimino CR, Fontanet HL, Cintron GB, Staffetti JF, Dunne PB, Sullivan KL. Heart failure in Parkinson's disease: analysis of the United States medicare current beneficiary survey. Parkinsonism Relat Disord. 2004; 10(7):417–20. [PubMed: 15465398]

Zhang Q, Bethmann C, Worth NF, Davies JD, Wasner C, Feuer A, Ragnauth CD, Yi Q, Mellad JA, Warren DT, et al. Nesprin-1 and -2 are involved in the pathogenesis of Emery Dreifuss muscular dystrophy and are critical for nuclear envelope integrity. Hum Mol Genet. 2007; 16(23):2816–33. [PubMed: 17761684]

Highlights

- *Drosophila* Ari-1 is required for nuclear localization via the LINC complex
- Parkin and Ari-1 are partially functionally redundant
- Human ARIH1 regulates the nuclear morphology of vascular smooth muscle cells
- Mutations in *ARIH1* are associated with aortic aneurysms

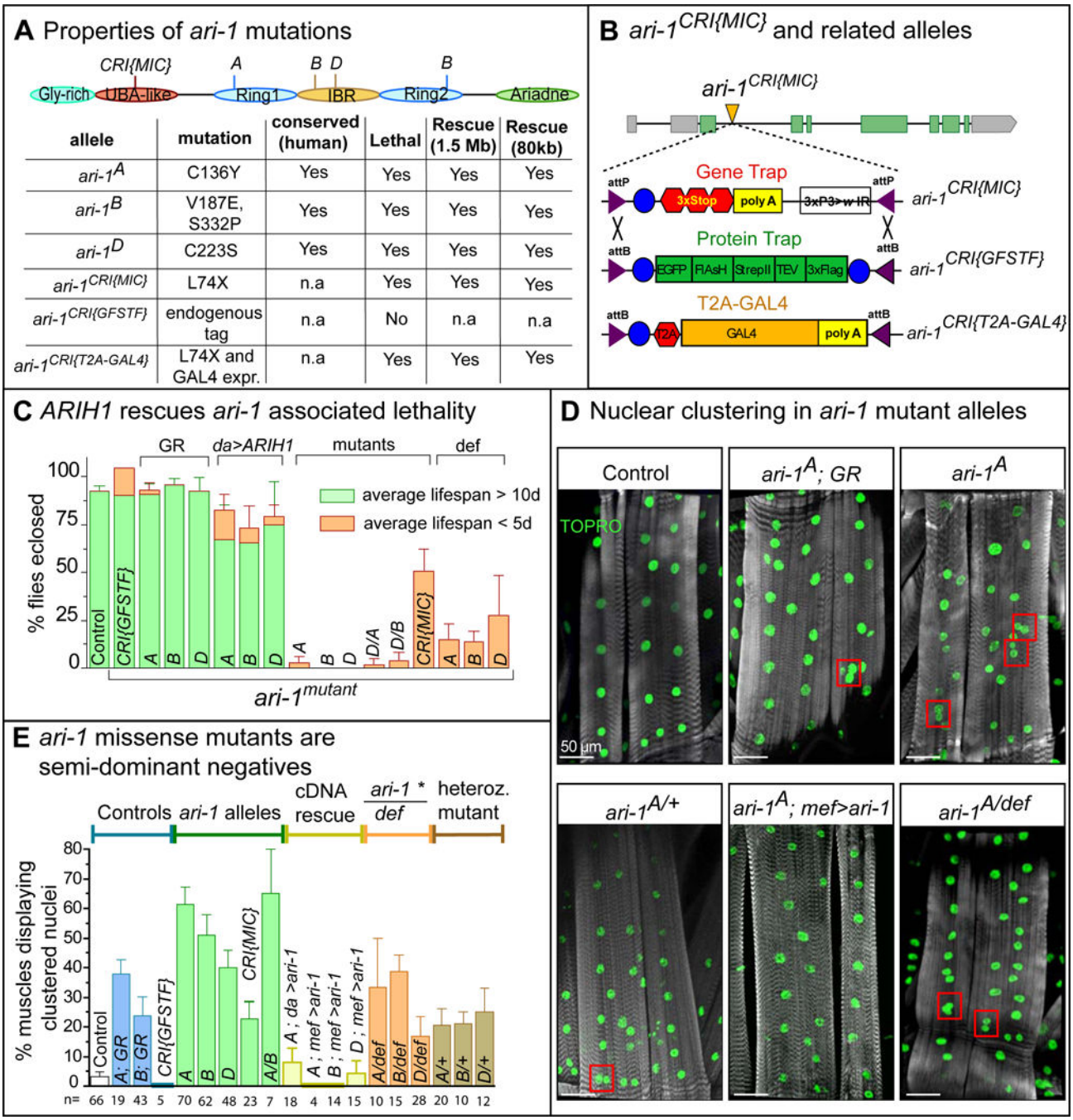

Figure 1. Loss of Ari-1 affects nuclear positioning in *Drosophila* muscles

(A) Protein domains: Gly-rich: glycine-rich, UBA-like: ubiquitin associated (UBA)-like, Ring1: first RING, IBR: in between RING, Ring2: second RING. Table describing characteristics of *ari-1* alleles used in this study. *ari-1*-associated lethality is rescued by duplications that cover the *ari-1* locus: *Dp1528* (1.5Mb, duplicated segment: X:17.79Mb… 18.98Mb) and the Pacman duplication *Dp(1;3)DC342* (80kb) (Venken et al., 2010).

(B) CRISPR-mediated integration of a Mi{MIC}-like cassette (CRI{MIC}) in *ari-1*'s first coding intron to generate *ari-1*$^{CRI\{MIC\}}$ (Gene Trap). The gene trap cassette was exchanged

with RMCE for a protein trap cassette (*ari-1*$^{CRI\{GFSTF\}}$) to tag Ari-1. We also exchanged the CRI{MIC} cassette for a T2A-GAL4 cassette, which functions as a gene trap that simultaneously induces GAL4 expression that mimics that of *ari-1* (*ari-1*$^{CRI\{T2A\text{-}Gal4\}}$).

(C) Graph displaying the percentage of animals that eclose and live a few (orange) or more than 10 (green) days. Control: *FRT19A*^{ISO}, isogenized parental strain used to generate *ari-1* mutants (Yamamoto et al., 2014); used as controls throughout this study unless indicated otherwise. GR: genomic rescue, Pacman duplication DC342. da>*ARIH1*: ubiquitous *ARIH1* expression (*daughterless-GAL4*). Def: deficiency *Df(1)BSC352*, uncovering the *ari-1* locus. Data shown as mean ± SD, n≥100 per genotype except for *ari-1*$^{D/A}$ (n=69) and *ari-1*$^{A,B\ or\ D\ /\ def}$ (n=50).

(D) Third instar larval body wall muscles stained for actin (phalloidin, gray) and nuclei (TOPRO, green). Red boxes mark examples of nuclei that touch each other. All muscles shown throughout study are third instar larval muscle 6, segment 3. Scale bar: 50 μm.

(E) Quantification of **(D)**. Graph displaying the percentage of muscles that show at least two touching nuclei. Mef: Mef2-GAL4, muscle-specific expression. Data shown are mean ± SD.

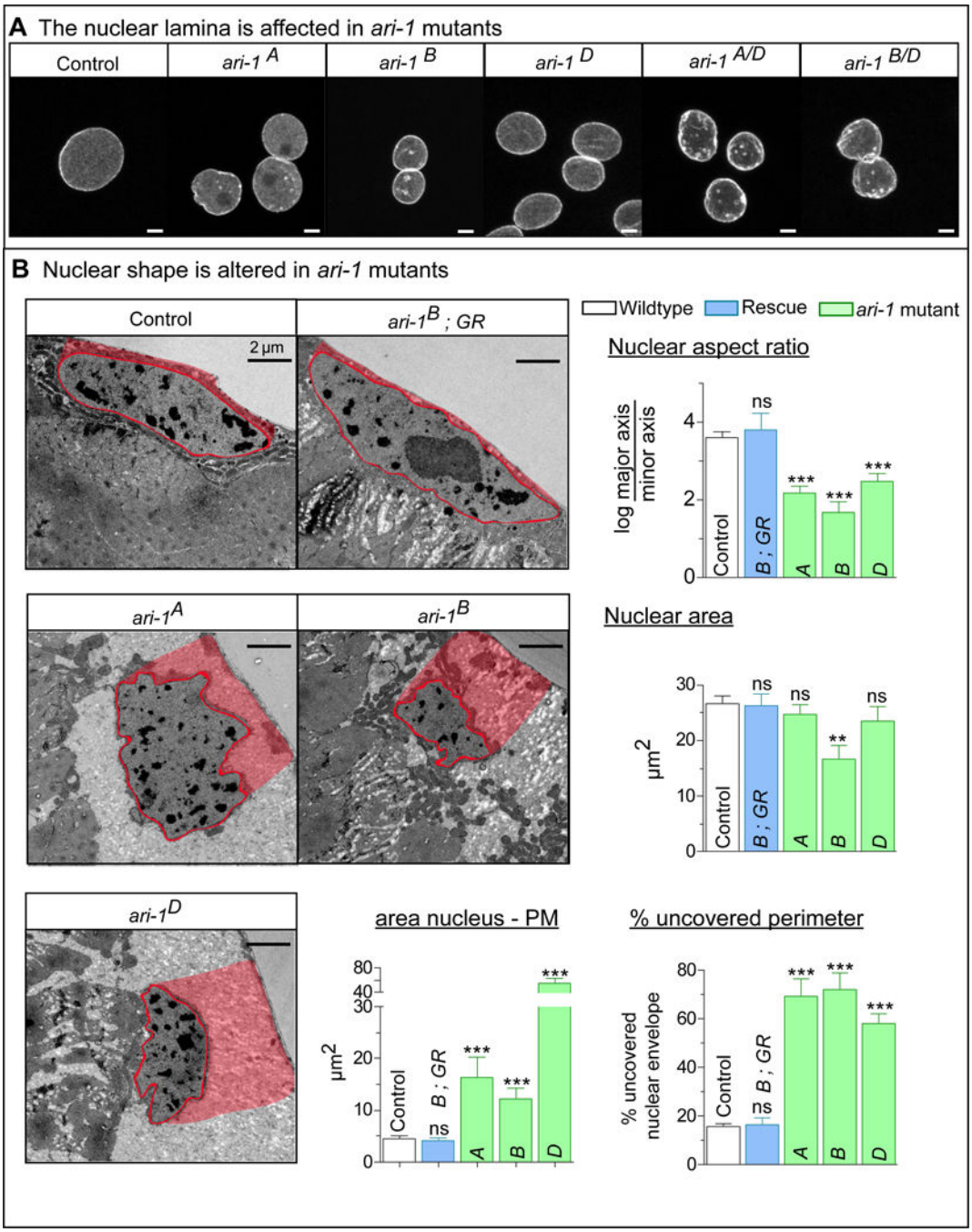

Figure 2. Nuclear morphology is compromised in *ari-1* mutants

(A) Muscle nuclei stained for LaminC. Scale bar: 5 µm

(B) Left: Electron micrographs of third instar myonuclei. Red outlines nuclei; Pink shades mark the area between the nucleus and the plasma membrane (area nucleus – PM). Right: Nuclear aspect ratio, (measure of ellipsoid shape); Nuclear area; % uncovered perimeter (percentage of the nuclear circumference that is not covered by mitochondria, cytoskeleton or plasma membrane); area nucleus - PM (area between nucleus and PM). Data from 3

animals per genotype, mean ± SEM. Statistical analysis: Unpaired t-tests. ns: non-significant, $p>0.05$; **: $p<0.001$; ***$p<0.0001$.

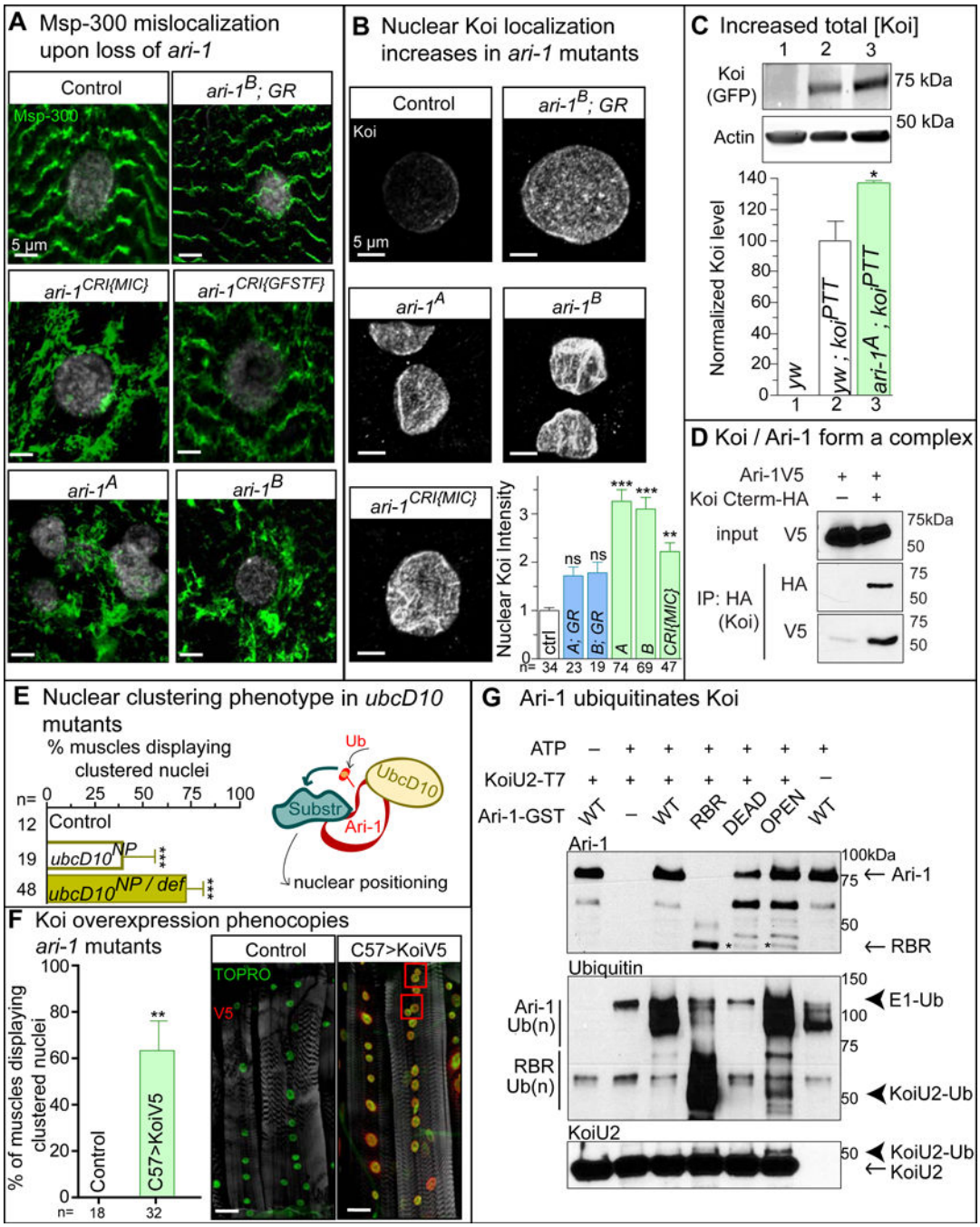

Figure 3. Ari-1 regulates the LINC complex and ubiquitinates Koi

(A) Larval muscles stained for Msp-300 (green, anti-Msp-300) and nuclei (white, DAPI). Scale bar: 5 µm.

(B) Myonuclei, stained for Koi (white). Scale bar: 5 µm. Bottom right: quantification of Koi intensity. Values are normalized to the average Koi intensity in controls. Error bars represent SEM values. Statistical analysis: One-way ANOVA with Tukey post-test. ns: non-significant, p>0.05; **: p<0.001; ***p<0.0001

(C) Top: Western blot (anti-GFP) of larval lysates of genotypes shown in the graph below. *koi*$^{P\{PTT\}}$ is a protein trap that labels 4/6 isoforms (Figure S3E). *yw* (*y*^{1}*w*);* negative control. Bottom: Quantifications of GFP, normalized to actin levels. Data shown are mean ± SD, n=3. Statistical analysis: unpaired t-test, * $p<0.05$

(D) Western blots of immunoprecipitations (IPs) of protein lysates of S2 cells expressing V5-tagged Ari-1 alone or in combination with HA-tagged Koi^{Cterm}.

(E) Left: Quantification of nuclear clustering in *ubcD10* mutants and control (*yw*). Data shown as mean ± SD. Statistical analysis: Unpaired t-test. ***: $p<0.0001$. Right: UbcD10 transfers ubiquitin (Ub) to Ari-1. Ub is subsequently transferred to the substrate.

(F) Left: Quantification of nuclear clustering in control (*w*; C57-GAL4) and *yw* overexpressing Koi (V5-tagged) in muscles with C57-GAL4. Right: Green: TOPRO (nucleus), White: Phalloidin (actin), Red: V5 (Koi). Data shown as mean ± SD. Statistical analysis: Unpaired t-test. **:$p<0.001$

(G) Western blots of (Top to Bottom) GST-tagged E3s (top), ubiquitin (visualized with streptavidin-HRP, middle), and T7-tagged KoiU2 (bottom). Arrows indicate unmodified proteins; arrowheads indicate ubiquitin-modified proteins. The protein identities of observed ubiquitin-positive smears in the ubiquitin blot are indicated to the left. * marks a non-specific band. WT-wild type Ari-1; RBR-Ring in between Ring domain of ARIH1; OPEN-full length, catalytically-active Ari-1; DEAD – full length Ari-1 containing OPEN and catalytically dead mutations.

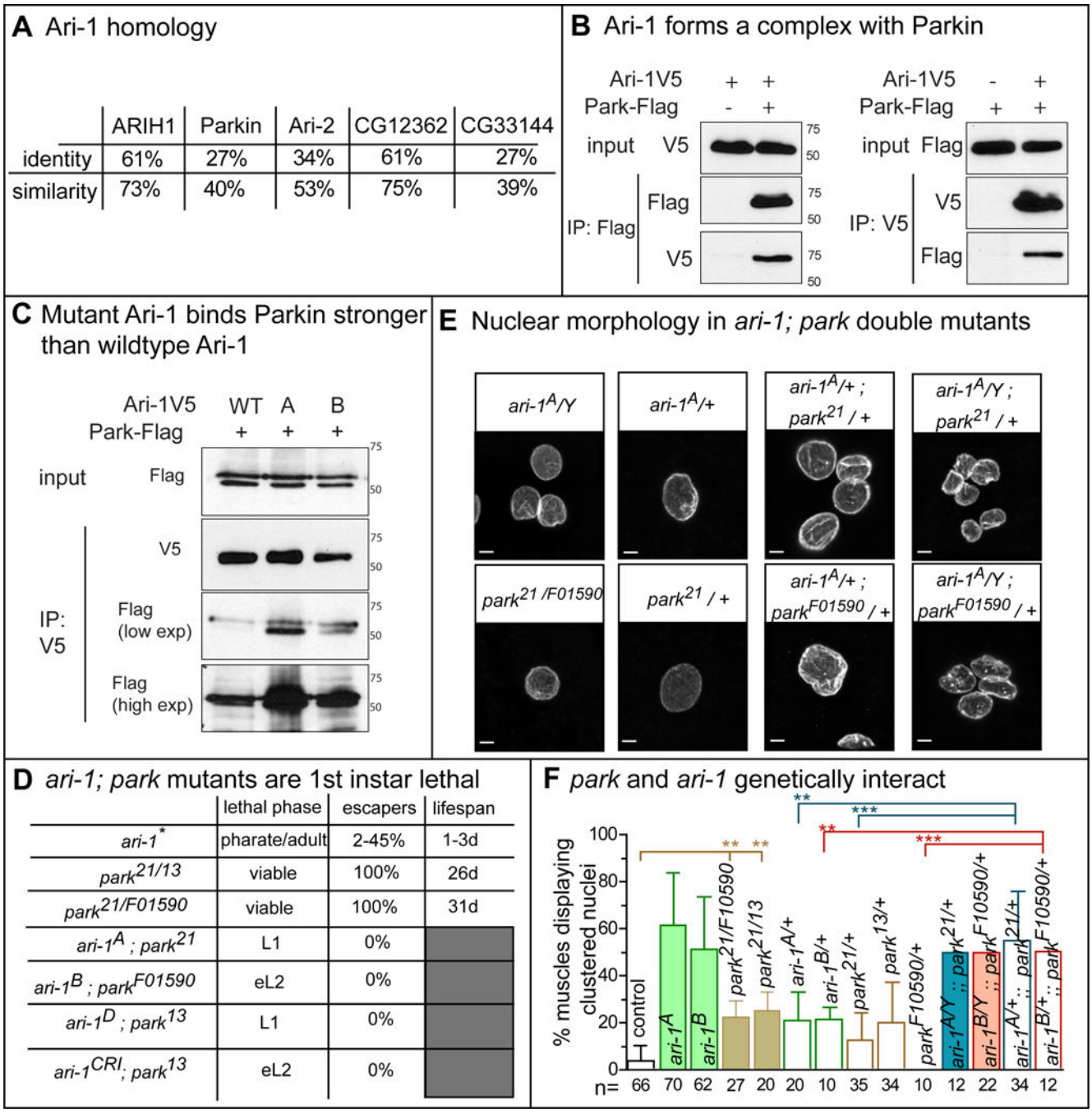

Figure 4. Ari-1 and Parkin (Park) genetically interact

(A) Protein homology of *Drosophila* Ari-1 with its human homolog (ARIH1), and other fly RBR proteins. Percentage of protein sequence identity and similarity are compared.

(B) Western blot of *Drosophila* S2 cell protein lysates. Left: Forward and reverse co-immunoprecipitation (co-IP) of Ari-1 (V5) and Parkin (Flag).

(C) Western blot of co-IP between Ari-1 and Parkin. Protein lysates obtained from *Drosophila* S2 cells that express V5-tagged wild type (WT), *ari-1*^{A} or *ari-1*^{B}, and Parkin (Flag).

(D) Comparison of lethal phase, percentage of escapers, and average lifespan in *ari-1* and *parkin* mutant backgrounds.

(E) Images displaying muscle nuclei stained for LaminC. Scale bar: 5 μm.

(F) Nuclear clustering analysis. Graph displaying the percentage of muscles that show at least two contacting nuclei. Data shown as mean ± SD. Statistical analysis: Unpaired t-tests compare *park* mutants to control. One-way ANOVA with Tukey post-test compare single heterozygous mutants (*ari-1*/+* or *park*/+*) to double heterozygous mutants (*ari-1*/+; park*/+*). ns: non-significant, $p>0.05$; **: $p<0.001$; ***: $p<0.0001$.

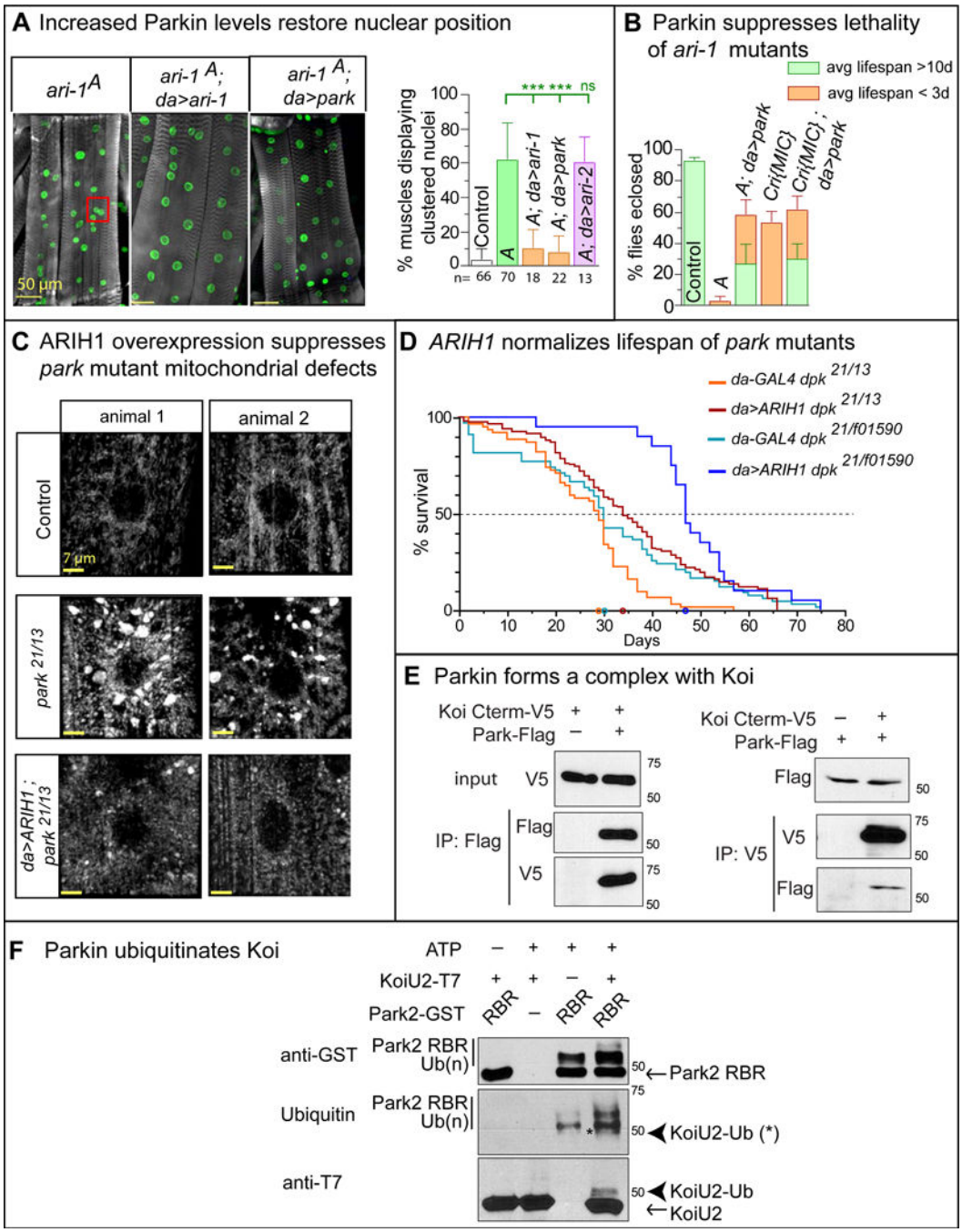

Figure 5. Ari-1 and Parkin (Park) functionally overlap

(A) Left: muscles stained for nuclei (DAPI, green) and actin (Phalloidin, white). Scale bar: 50 µm. Right: Graph of percentage of muscles that display at least two contacting nuclei. Data shown as mean ± SD. Statistical analysis: Unpaired t-test, all genotypes (except for control) are compared to *ari-1*^{A}. ns: non-significant, p>0.05; **: p<0.001; ***: p<0.0001. **(B)** Graph of percentage of adult flies that eclose and survive past three days (green) or eclose and have an average lifespan of three days (orange). ≥250 animals were analyzed per genotype. Data shown as mean ± SD.

(C) Confocal images of the mitochondrial network in third instar muscles, stained for the mitochondrial complex V subunit ATP5A (white). Scale bar: 7 μm.
(D) Survival curves. The intersection between the dashed line and the survival curves represents the 50% lifespan (open circles on the X-axis). Orange and light blue curves are controls for red and dark blue curves respectively.
(E) IPs of *Drosophila* S2 cells, expressing Koi^{Cterm} (V5) and / or Parkin (Flag). Forward and reverse co-IPs are shown.
(F) Western blots (Top to Bottom): GST-tagged Parkin RBR (top), ubiquitin (visualized with streptavidin-HRP, middle), and T7-tagged KoiU2 (bottom). Arrows indicate unmodified proteins; arrowheads indicate ubiquitin-modified proteins. * marks the exact MW of KoiU2-Ub, which is partially masked by active, auto-ubiquitinated Park2 RBR Ub(n) (Ubiquitin blot). The protein identities of observed ubiquitin-positive smears in the ubiquitin blot are indicated to the left.

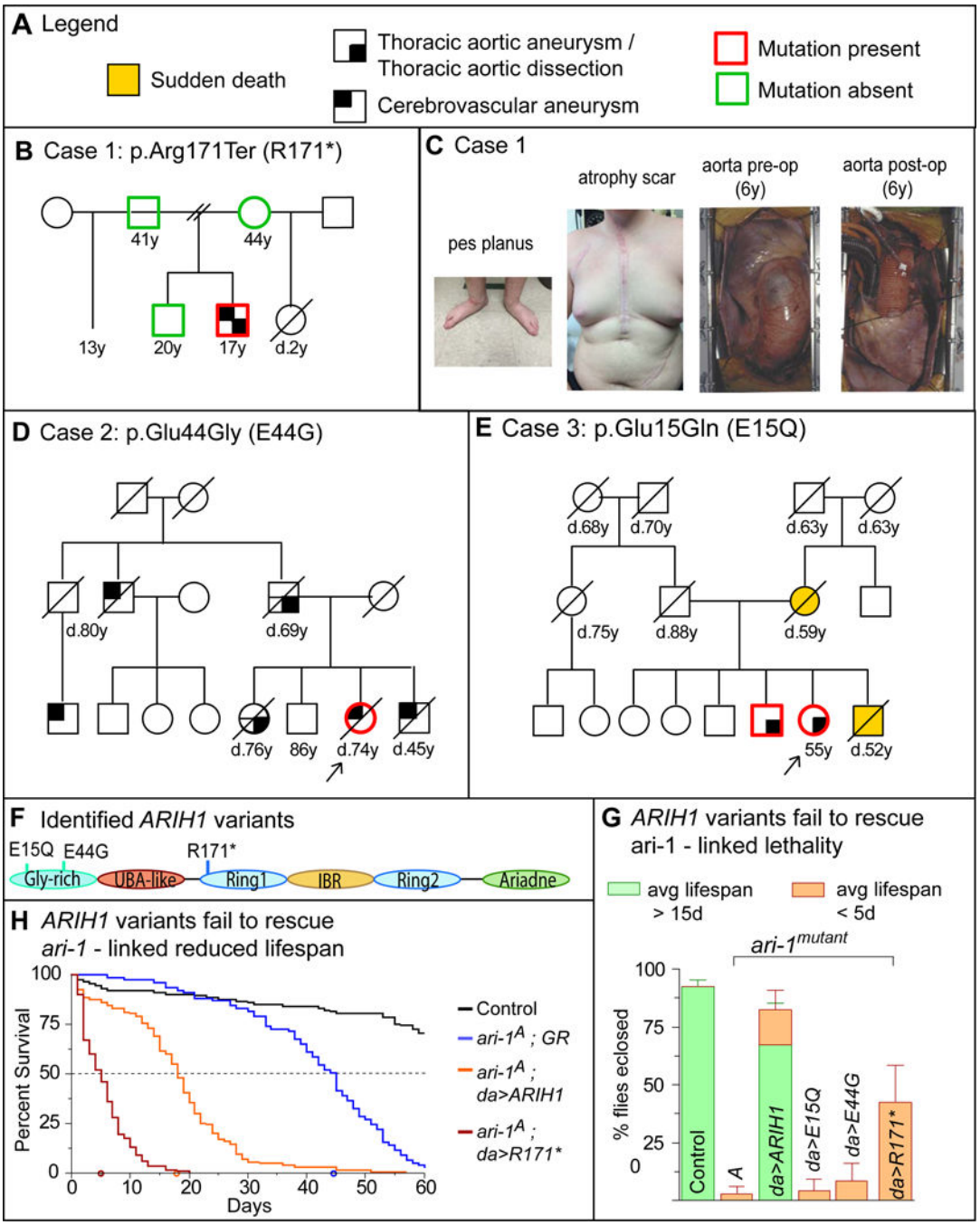

Figure 6. *ARIH1* variants in patients with aortic aneurysm

(A) Figure legend for **(B)**, **(D)** and **(E)**. Pedigrees of the three cases with *ARIH1* variants are shown in panels B, D and E. Family members indicated with partially dark-filled shapes have aortic aneurysm and/or cerebrovascular aneurysms. Family members indicated with orange-filled shapes experienced sudden death. Family members indicated with red or green boxes underwent exome sequencing; red boxes indicate the presence of a variant in *ARIH1* whereas green boxes indicate the absence of an *ARIH1* variant. Ages at last follow up or death are indicated under each symbol. Panel **(C)** shows physical characteristics noted in

Case 1: atrophic scars, significant pes planus and two intraoperative images of Case 1's aorta before and after the first aneurysm repair at age 6. Informed consents were obtained from all subjects.

(F) Model displaying ARIH1's protein domain structure and localization of the three identified variants. Two missense variants (E15Q and E44G) were identified in the N-terminal glycine-rich domain, whereas one nonsense variant (R171*) was identified in the beginning of the RING1 domain.

(G) Graph displaying the percentage of adult flies that eclose and live longer than 15 days (green) or less than 5 days (orange). ≥150 animals were analyzed per genotype, except for *ari-1^{A}; da>E44G* (n=49). Data are mean ± SD.

(H) Survival curves. The intersection between the dashed line and the survival curves represents the 50% lifespan of each genotype (open circles on the X-axis).

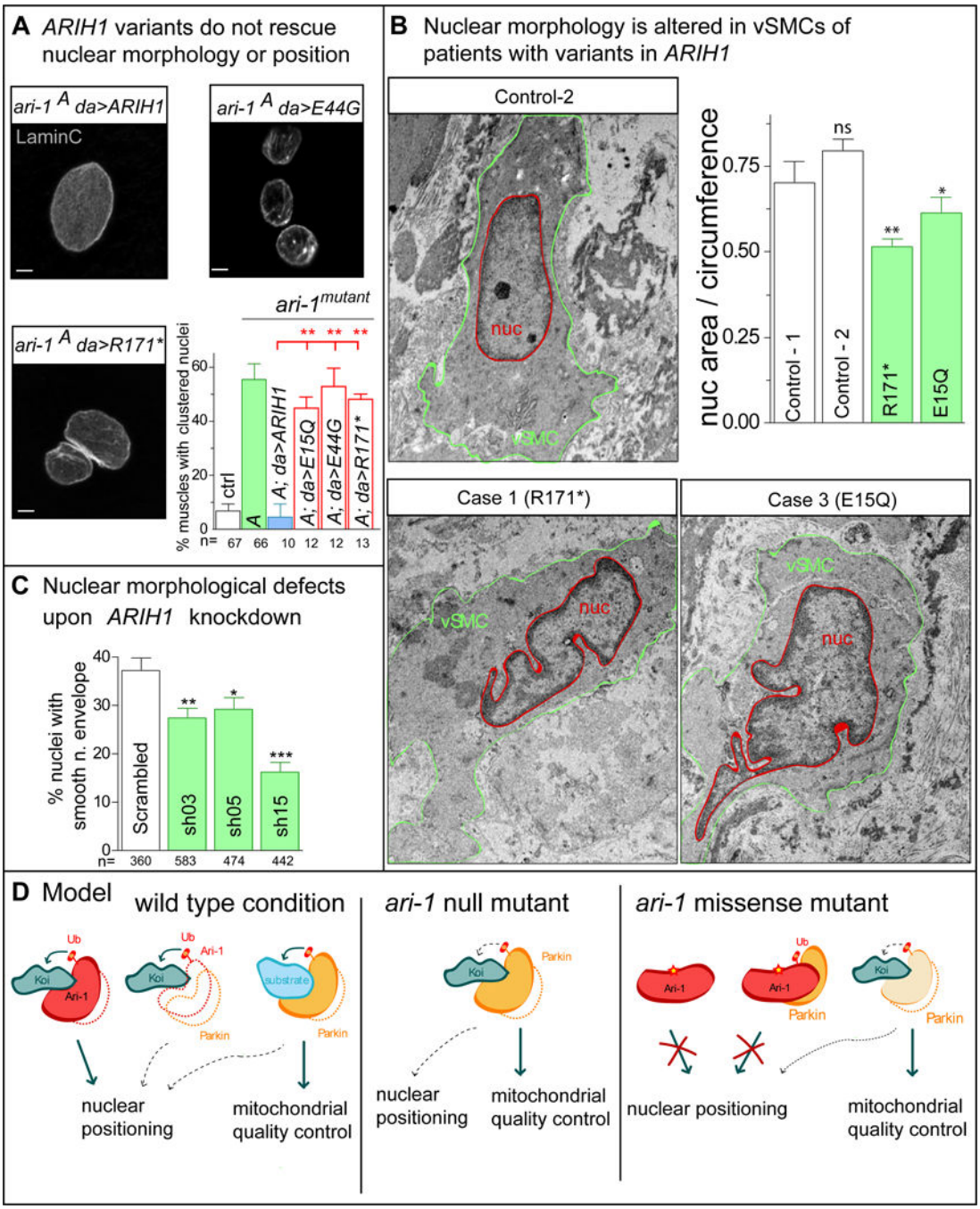

Figure 7. Loss of *ARIH1* alters nuclear morphology

(A) Images displaying nuclear envelope morphology (laminC, white) of myonuclei in third instar larvae. Scale bar: 5 μm. Bottom right: Quantification of the percentage of muscles that show at least two contacting nuclei. Data are represented as mean ± SEM. Statistical analysis: unpaired t-test comparing *ari-1^{A} ; da>ARIH1* with *ari-1^{A} ; da>ARIH1^{mutant}*. **: p<0.001

(B) TEM images of aortic patient tissue (R171* and E15Q). vSMCs are outlined in green, nuclei are outlined in red. Top right: Graph displaying the ratio of nuclear area to nuclear

circumference (n≥35 per tissue sample). Data are represented as mean ± SEM. Statistical analysis: Unpaired t-test compared to Control-1. ns: non-significant, p>0.05; *: p<0.01; **: p<0.001

(C) Quantification of the percentage of vSMCs containing round, smooth nuclei upon transfection with scrambled or *ARIH1* shRNA (03, 05 and 15, GE Dharmacon). n≥350 cells per genotype. Statistical analysis: unpaired t-test. *: p<0.01; **: p<0.001; ***p<0.0001

(D) Working model. (Left) In wildtype conditions, Ari-1 regulates nuclear positioning and is aided by Parkin. Parkin's main function is to regulate mitochondrial quality control. (Middle) In the absence of *ari-1*, Parkin assumes some regulation of nuclear positioning. (Right) Mutant Ari-1 acts in a dominant negative fashion and affects Parkin's ability to compensate for nuclear positioning, leading to a more severe phenotype. Not all Parkin complexes are affected by Ari-1 mutant proteins, allowing Parkin to sustain mitochondrial quality control.